BRITISH ANTARCTIC SURVEY

SCIENTIFIC REPORTS

No. 88

A SIMPLE EMPIRICAL METHOD FOR ESTIMATING THE HEIGHT AND SEMI-THICKNESS OF THE *F2*-LAYER AT THE ARGENTINE ISLANDS, GRAHAM LAND

By

J. R. DUDENEY, B.Sc., Ph.D.

British Antarctic Survey Atmospheric Sciences Division
at S.R.C. Appleton Laboratory, Slough

LONDON: PUBLISHED BY THE BRITISH ANTARCTIC SURVEY: 1974
NATURAL ENVIRONMENT RESEARCH COUNCIL

BRITISH ANTARCTIC SURVEY SCIENTIFIC REPORTS: No. 88

A SIMPLE EMPIRICAL METHOD FOR ESTIMATING THE HEIGHT AND SEMI-THICKNESS OF THE *F2*-LAYER AT THE ARGENTINE ISLANDS, GRAHAM LAND

By

J. R. DUDENEY, B.Sc., Ph.D.

British Antarctic Survey Atmospheric Sciences Division
at S.R.C. Appleton Laboratory, Slough

(Manuscript received 13th February, 1974)

ABSTRACT

A CRITICAL analysis of the basis for simple relationships between *hpF2* and *M(3000)F2* is made and a method is suggested whereby an accurate set of equations, including the effects of the Earth's magnetic field, could be derived.

The principles underlying simple empirical methods for estimating *hmF2* are discussed and a critical review of previous work in this field given.

A simple method is described for modifying the *M(3000)F2* factor such that the new factor, when used in the Shimazaki (1955) equation, gives a very good estimate of *hmF2*. It is demonstrated that the method, which uses only the *M(3000)F2* factor and the ratio of *foF2* to *foE*, is valid for all epochs of the solar cycle and all seasons. Further, although the analysis is based on data from only one observatory, the techniques developed have a much wider application.

An empirical method for estimating *ymF2* once *hmF2* is known is mapped out, but shortcomings in the precision of this method are pointed out.

CONTENTS

I. INTRODUCTION

THERE is a continuing need for reliable but readily available values of the true height of the maximum electron concentration of the *F2*-layer (symbol *hmF2*) amongst theoreticians and propagation engineers. This need will grow during the next few years because of the demands of the International Magnetospheric Study. This report describes a method of deducing accurate values (normally better than $\pm$ 5 per cent) of *hmF2* using only those parameters routinely scaled from ionograms. The method is based on ionospheric observations made at the British Antarctic Survey geophysical observatories at the Argentine Islands (lat. 65°15′S., long 64°16′W.) and Port Lockroy (lat. 64°49′S., long. 63°30′W.). Geophysically, the two sites are equivalent and throughout this report data from both will be referred to as Argentine Islands data without further comment.

1. *Vertical incidence sounding*

The classical method of obtaining information about the ionosphere is to employ radio waves of a suitable frequency as a probe. A plasma which varies slowly with height will totally reflect a radio wave of frequency f, incident normally, when the ion concentration within the plasma (N) satisfies the equation

$$N = \left(\frac{\pi m_e}{e^2}\right) f^2. \tag{1}$$

It is often convenient to use the resonant frequency of the plasma (f_N) at the point of reflection

$$f_N = (Ne^2/\pi m_e)^{\frac{1}{2}}. \tag{2}$$

If the source of radio waves is pulsed, the time of flight of the pulses can be measured.

These principles are embodied in an instrument called an *ionosonde*. This consists of a transmitter whose operating frequency is swept automatically from about 0·5 to 30 MHz (typically taking about 1 to 5 min.) and whose output feeds a wide-band aerial designed to transmit maximum power vertically upwards. A sensitive receiver is held in tune with the transmitter and records both the outgoing and returning pulses. These are displayed on a cathode-ray tube whose time base also shows subsidiary calibration pulses from which the time of flight can be determined. It is usual to divide the time of flight by 2 and multiply by the speed of light *in vacuo* to give the *virtual height* of reflection h'. As will be seen below, this virtual height is only loosely related to the *true height* of reflection, h, because the ionosphere is not a simple mirror in the optical sense but a thick refracting medium.

The echoes displayed on the c.r.t. are normally photographed by winding a film past the face of the tube. This gives a continuous record of h' as a function of f up to the frequency which penetrates the ionosphere. The resultant picture is called an $h'(f)$ profile or *ionogram.*

2. *The relation between virtual height and true height*

Suppose a wave of the form $E = \epsilon \exp\{i(\omega t - kx)\}$ is propagated vertically upwards into a horizontally stratified ionosphere. The group velocity, u, decreases with increasing electron concentration and becomes a minimum at the point of reflection (zero if the collision frequency is negligible). The total time of flight, t, is simply given by the integral

$$t = 2\int_0^h \frac{dh}{u},$$

where h is the height of reflection.

From this it follows that virtual height is defined by

$$h' = \int_0^h \frac{c}{u} dh.$$

But c/u is the group refractive index μ' so that

$$h' = \int_0^h \mu' \mathrm{d}h. \tag{3}$$

The relationship between μ' and μ, the phase refractive index, is given by

$$\mu' = \mu + \omega \frac{\mathrm{d}u}{\mathrm{d}\omega}. \tag{4}$$

Magneto-ionic theory (Ratcliffe, 1962) gives the phase refractive index in terms of the parameters of the plasma and the probing frequency. The general dispersion equation involves the plasma frequency, gyro frequency, dip angle and collision frequency in a complex manner. However, for the simple case, where the Earth's magnetic field and the effects of collisions are neglected

$$\mu^2 = 1 - \left(\frac{\omega_N}{\omega}\right)^2 = 1 - \left(\frac{f_N}{f}\right)^2. \tag{5}$$

Substituting this in Equation (4) leads to the simple relation, $\mu\mu' = 1$. Thus, for this special case, Equation (5) can be used directly in Equation (3), giving a well-known standard equation.

The general expression for h' (Equation (3)) can also be written in terms of the plasma frequency to give

$$h'(f) = \int_0^f \mu' \left(\frac{\mathrm{d}h}{\mathrm{d}f_N}\right) \mathrm{d}f_N + h(o), \tag{6}$$

where $h(o)$ is the base height of the ionosphere (at which $\mu' = 1$).

In principle, any given $h'(f)$ profile can be converted into a true height versus frequency profile by inverting Equation (6) and integrating the resultant expression numerically using the recorded values of h' for various suitable values of f. Equation (2) then gives the true height versus electron concentration profile ($N(h)$ profile).

Before the advent of digital computers, the enormous computational difficulties involved in this numerical solution severely curtailed its usefulness. Nowadays, with powerful computers available, it is possible to invert the integral even when using the complete dispersion equation. However, several major practical problems make it difficult to obtain accurate profiles. These problems may be summarized:

i. The integration requires virtual-height information from zero plasma frequency up to the critical frequency of the densest layer. In practice, several parts of the $h'(f)$ curve may be missing.
ii. A unique numerical solution only exists if the $N(h)$ profile is monotonic.
iii. The virtual height may become infinite at a critical frequency, causing difficulty in evaluating the area under the curve.

The solutions of these difficulties fall into two groups:

i. Use of assumed model ionization distributions where data are missing.
ii. Use of ordinary and extraordinary ray traces to estimate the effect of the missing parts of the pattern.

In practice, both techniques have only limited usefulness.

Even with the aid of computers, numerical analysis is still expensive and time consuming. There are always practical difficulties associated with the use of any computer facility. Furthermore, many precision measurements of h' and f must be made from the original ionogram, a particularly laborious task. It is thus usually beyond the average research worker's resources to obtain more than a small sample of profiles, so that their use is limited to special studies of isolated events or for calibration of larger groups of less accurate data.

These difficulties have maintained interest in the so-called "model" methods. For these, the $N(h)$ profile is assumed to be given by a known analytical expression whose constants are obtained by matching the theoretical $h'(f)$ profile, found by integrating Equation (6), with the observed profile. The constants of the model are chosen to represent the heights of maximum electron concentration and the thicknesses of the main ionospheric layers. Since the peak heights and thicknesses are important in the science of the ionosphere, model methods have been developed to give these parameters explicitly in terms of parameters readily measured from ionograms. The method of estimating *hmF2* to be developed in this report is of this

general type. However, a further criterion will be that only ionospheric parameters routinely published by the observatories should be required so that access to original ionograms when using the method will not be necessary. Also numerical $N(h)$ analysis will be used to calibrate the model.

II. THE PROPERTIES OF A PARABOLIC LAYER

1. *Early work: the equivalent parabolic layer*

A very simple approach to the problem of estimating *hmF2* is to assume that the ionosphere consists only of an *F2*-layer whose profile is a simple parabola. If then, the effects of collisions and of the Earth's magnetic field are neglected, a simple relationship between h' and h can be derived. Booker and Seaton (1940) and Appleton and Beynon (1940) were among the first workers to discuss methods of estimating the height of maximum of such a layer. Their argument will be considered in some detail, but the current nomenclature will be used.

Consider a parabolic layer whose maximum electron concentration is *No* at height *hp*. Suppose the semi-thickness is *yp* so that the base height is $ho = hp - yp$. It follows that

$$N = No\left[1-\left(\frac{hp-h}{yp}\right)^2\right]. \tag{7}$$

If the minimum frequency which just penetrates the layer (*critical frequency*) is *fo*, then from Equations (1) and (7) frequency f is reflected when

$$f^2 = fo^2\left[1-\left(\frac{hp-h}{yp}\right)^2\right]. \tag{8}$$

Integrating Equation (6) using Equations (5) and (8)

$$h'(f) = \frac{yp}{2}\frac{f}{fo}\log_e\left[\frac{fo+f}{fo-f}\right]+ho. \tag{9}$$

Define a function $\phi(x)$ as

$$\phi(x) = \frac{x}{2}\log_e\left[\frac{1+x}{1-x}\right]-1, \tag{10}$$

where $x = f/fo$.

Substituting Equation (10) in (9) noting that $hp = ho+yp$, it follows that

$$hp = h'(f)-yp\,\phi(x). \tag{11}$$

hp and *yp* can be calculated from any pair of frequencies just by measuring the corresponding values of h'. The accuracy of the results depends on the frequency separation and on any deviations of the layer structure from strictly parabolic shape. Also, $\phi(x)$ is a very rapid function of x when $x \to 1$, so that small errors in x cause disproportionate errors in the deduced value of *yp*. These can be reduced by using Appleton and Beynon's method of plotting h' as a function of $\phi(x)$ and drawing the best straight line. Alternatively, a family of $h'(f)$ patterns can be computed for different values of *yp* and these matched to the observed profile. In both cases *yp* is critically dependent on the accuracy with which the critical frequency is known.

Note that $\phi(x) = 0$ at $x = 0{\cdot}834$, so that $hp = h'$ at $x = 0{\cdot}834$. Thus, *hp* can be determined by just one measurement from the ionogram. In practice, the effect of underlying ionization is to increase the value of h' at $0{\cdot}834fo$ above the true value of *hp*. This is usually negligible at night but can be serious in daytime.

The inclusion of the Earth's magnetic field (B) modifies the form of $\phi(x)$ to $\phi'(x)$ where the latter depends upon magnetic dip and the ratio of f_B to *fo* (f_B = gyro frequency). The peak height can still be found by putting $\phi'(x) = 0$, but now the value of x to satisfy this equation (x_c, say) varies with dip, I, and f_B/fo. Using the published computed tables of $\phi'(x)$ (Becker, 1960), it can be shown that x_c decreases smoothly from $0{\cdot}834$ both with increasing I (constant f_B/fo) and increasing f_B/fo (constant I). A decrease in x_c means a decrease in h', so the error, Δh, incurred by neglecting the B-field is always positive. The tables also indicate that Δh can be expressed as a fraction of *yp*, *ayp* say, where the factor "*a*" is a function of x_c alone, increasing as the latter decreases. At a particular location, "*a*" is uniquely related to *fo* since I and f_B are fixed. For the Argentine Islands, where $I = 60°$ and f_B is $1{\cdot}15$ MHz, the form of the variation is

shown in Fig. 1. Note that for a typical *yp* of 100 km. Δh is quite small, of the order of 6 to 25 km. depending on *fo*. This apparent lack of sensitivity to the *B*-field can be explained by considering the variation of μ' with x (see, for example, Ratcliffe (1962, p. 104)). The no-field value of μ' is greater than the value with the field when x is small but less when x is large, so that a partial compensation occurs in the integral near $\phi'(x) = 0$. The same argument applies generally; neglect of the *B*-field seldom affects the value of *hm* greatly but it will cause distortions to the profile shape. It is thus often adequate to neglect the *B*-field when computing *hp*.

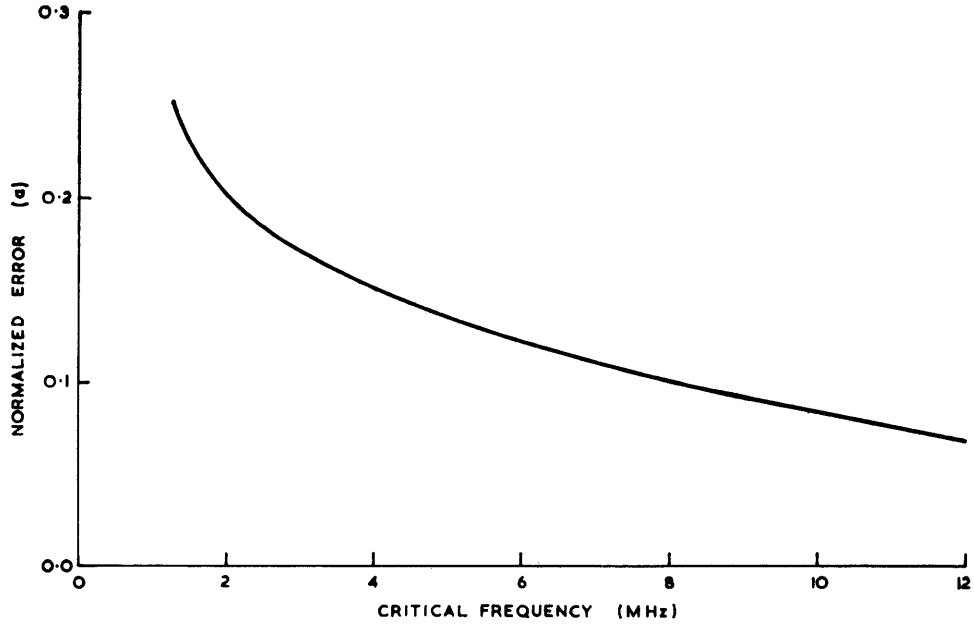

FIGURE 1

The error, "*a*", in *hp*, expressed as a fraction of *yp*, incurred by assuming the no-field approximation $hp = h'(f = 0{\cdot}834fo)$. These results apply for $I = 60°$ and $f_B = 1{\cdot}15$ MHz.

2. *The relationship between hp and M(3000)F2*

The relation between the maximum usable frequency, *MUF*, which can be reflected to a given distance and the critical frequency of the reflecting layer, *fo*, depends on distance, the height and thickness of the reflecting layer, and to a lesser extent on the presence of underlying ionization. For practical reasons, it has been agreed internationally to adopt the ratio of *MUF*/*fo* for a standard distance of 3,000 km. as a standard communications parameter. This is called the *M(3000)* factor and is calculated according to an agreed semi-empirical relation. A clearer insight into the significance of *M(3000)* can be obtained from a study of the relation between *M(3000)* and *hp*. The classical work on this subject was carried out by Appleton and Beynon (1940) and the present investigations will be based on their analysis.

3. *The case of the thin layer*

a. *For a flat Earth.* Consider Fig. 2a. Suppose the refractive index of the layer at the point of reflection is μ, then from Snell's law

$$\mu^2 = \sin^2 i_0.$$

Suppose the sounding frequency on the oblique path is f and the critical frequency is *fo*; it follows that

$$\mu^2 = \sin^2 i_0 = 1 - \frac{fo^2}{f^2}.$$

But
$$\tan i_0 = D/2ho,$$

therefore

$$\left(\frac{fo}{f}\right)^2 = 1/\left\{\frac{D^2}{4ho^2} + 1\right\}.$$

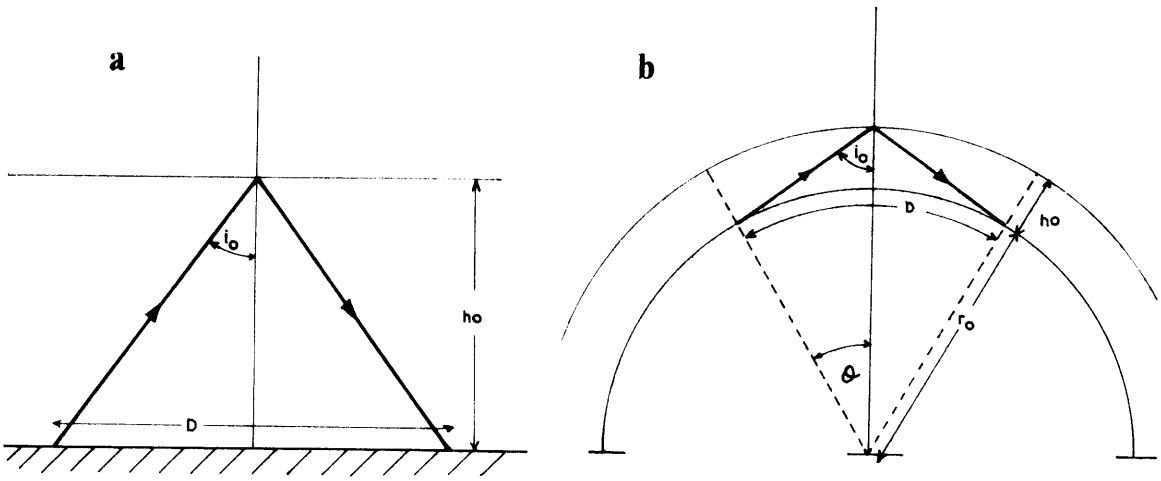

FIGURE 2

a. Oblique propagation: thin ionosphere and flat Earth.
b. Thin ionosphere and curved Earth.

If f is taken to be the maximum usable frequency, then x equals f/fo, the MUF factor for a range D.

Thus,
$$x^2 = \frac{D^2}{4ho^2} + 1,$$

hence
$$ho = \frac{D}{2(x^2-1)^{\frac{1}{2}}}.$$

For the case of propagation to $D = 3{,}000$ km., $x = M$, the $M(3000)$ factor and

$$ho = \frac{1500}{(M^2-1)^{\frac{1}{2}}}. \tag{12}$$

b. *Curved Earth.* Referring to Fig. 2b, $D = 2r_0\theta$ and

$$\cos^2 i_0 = \frac{(ho + r_0 - r_0 \cos\theta)^2}{(ho + r_0 - r_0\cos\theta)^2 + r_0^2 \sin^2\theta}.$$

Since θ is always small,

$$\frac{fo^2}{f^2} = \cos^2 i_0 = \frac{(ho + r_0\,\theta^2/2)^2}{(ho + r_0\,\theta^2/2)^2 + r_0^2\theta^2}.$$

Substituting for θ and taking f as the MUF,

$$\frac{1}{x^2} = \frac{(ho + D^2/8r_0)^2}{(ho + D^2/8r_0)^2 + D^2/4}.$$

Re-arranging for ho,

$$ho = \frac{D}{2(x^2-1)^{\frac{1}{2}}} - \frac{D^2}{8r_0}.$$

Then for $D = 3{,}000$ km.

$$ho = \frac{1500}{(M^2-1)^{\frac{1}{2}}} - 176. \tag{13}$$

Comparing Equation (13) with (12), note that the effect of curvature is simply to reduce ho by a fixed factor. Assuming $1 \gg 1/M^2$, Equation (13) can be simplified to

$$ho = \frac{1500}{M} - 176. \tag{14}$$

This equation is remarkably similar to the Shimazaki result for a thick layer ($hp = 1490/M - 176$), which will be discussed later.

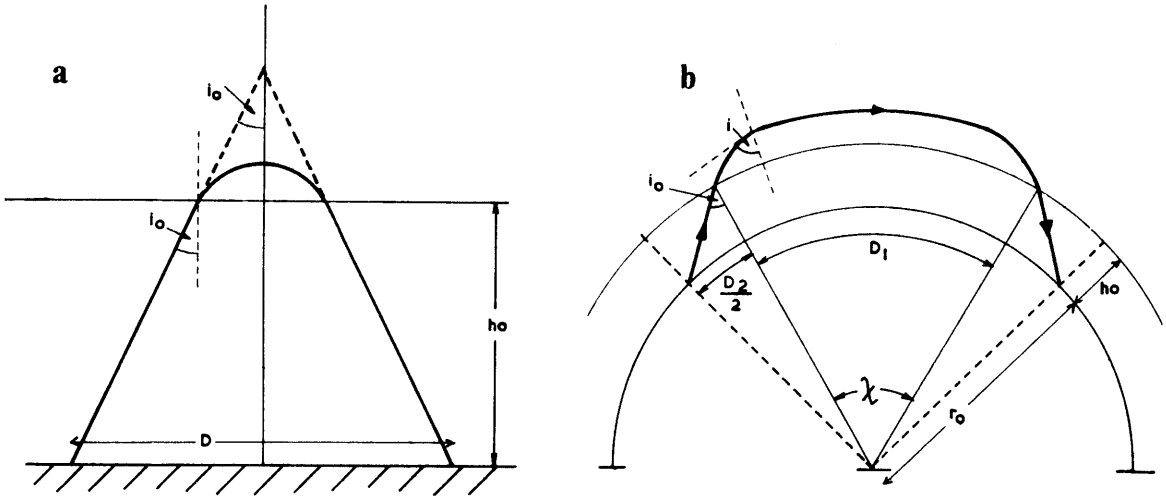

FIGURE 3
a. Flat Earth and thick ionosphere.
b. Curved Earth and thick ionosphere.

4. *The case of a thick parabolic layer*

a. *For a flat Earth.* Consider a parabolic layer of semi-thickness *yp* and base height *ho*. Suppose the critical frequency of the layer is *fo* and the operating frequency on the oblique path is *f*. Referring to Fig. 3a and applying Martyn's theorem, the equivalent path *P'* of the ray is given by

$$D = P' \sin i_0; \tag{15}$$

also for a ray traversing a parabolic layer,

$$P' = yp \frac{f}{fo} \log_e \left[\frac{fo+f\cos i_0}{fo-f\cos i_0}\right] + \frac{2\,ho}{\cos i_0}. \tag{16}$$

In Equation (16) the first term represents the equivalent path within the layer and the second term the path between ground and ionosphere. Eliminating *P'* from Equations (15) and (16) gives

$$D = yp \frac{f}{fo} \sin i_0 \log_e \left[\frac{1+f/fo\cos i_0}{1-f/fo\cos i_0}\right] + 2ho \tan i_0. \tag{17}$$

The turning point $\frac{dD}{di_0} = 0$ at constant *yp* and *ho* gives the relation between f/fo and i_0 such that $f = f_{MUF}$ and $f/fo = x$, the *MUF* factor. Differentiating Equation (17) and equating to zero gives

$$2\tan^2 i_0 \left[\left(\frac{x'^2}{1-x'^2}\right)\frac{yp}{ho} - 1\right] = \frac{yp}{ho} x' \log_e \left[\frac{1+x'}{1-x'}\right] + 2, \tag{18}$$

where $x' = x\cos i_0$.

Equations (17) and (18) contain the relationship between *hp* and *x* but this cannot be expressed analytically. It is possible to solve them for *hp* and *x* at fixed *D* and *yp*/*ho* by numerical methods; however, this will not be done for the flat Earth case, since this approximation is inadequate for a range of 3,000 km.

b. *Curved Earth.* In the curved Earth case, Martyn's theorem no longer applies and a simple expression linking the equivalent path with the ground range (such as Equation (15)) is no longer possible. Referring to Fig. 3b, it is now necessary to integrate along the path in the ionosphere to obtain χ and hence the part range D_1.

Let *i* be the angle the ray makes with the normal at any point along the path at a distance *r* from the centre of the Earth. Then, according to Bouguer's rule

$$\mu r \sin i = \mu_0 r_1 \sin i_0 = (r_0+ho)\sin i_0,$$

where $r_1 = r_0+ho$ and $\mu_0 = 1$.

Thus

$$\tan i = \frac{\sin i}{(1-\sin^2 i)^{\frac{1}{2}}} = \frac{r_1 \sin i_0}{(\mu^2 r^2 - r_1^2 \sin^2 i_0)^{\frac{1}{2}}}.$$

From Fig. 3b it is clear that $\tan i = r\frac{d\chi}{dr}$. Therefore $d\chi = \frac{dr}{r}\tan i$, from which,

$$\chi = \int \frac{r_1 \sin i_0}{r(\mu^2 r^2 - r_1^2 \sin^2 i_0)^{\frac{1}{2}}}\, dr. \tag{19}$$

The use of a parabolic $N(h)$ distribution to give μ from Equation (5) results in an intractable integral. However, using the approximation $ho/r_0 \ll 1$, Appleton and Beynon were able to solve Equation (19) to obtain the ionospheric part range D_1. With some further geometrical approximations for D_2, their final result was

$$D = \frac{r_0(x^2-x'^2)^{\frac{1}{2}}}{r_0+ho}\, yp \log_e \left[\left\{1-\frac{yp\,(x^2-x'^2)}{r_0+ho}+x'\right\}\Big/ \left\{1-\frac{yp\,(x^2-x'^2)}{r_0+ho}-x'\right\}\right] + 2r_0 \cot i_0 \left[1-\left\{1-\frac{2ho\tan^2 i_0}{r_0}\right\}^{\frac{1}{2}}\right], \tag{20}$$

where $x' = x\cos i_0$.

As before, equating dD/di_0 to zero will give the variation of x with i_0 independent of D. However, Appleton and Beynon showed that the resultant expression produced values only marginally different from those obtained from Equation (18) and concluded that this equation was adequate.

Equations (20) and (18) can be solved numerically to give the variation of hp with x for particular values of D and yp/ho. A computer program has been written to perform this task. This program has been used to solve the special case of $D = 3{,}000$ km. for a range of values of yp/ho between 0·1 and 1·0. The results of these calculations are shown in Fig. 4. In this figure, M has been plotted as a function of yp/ho for a number of values of hp (in the manner of Appleton and Beynon). Equation (13) was used to obtain values of M at $yp/ho = 0{\cdot}0$. Fig. 4 indicates that hp may have some functional link with $M(3000)$ and that this function will be substantially independent of yp/ho for yp/ho greater than 0·4. Equations (12) and (13) suggest that hp could be a function of $1/(M^2-1)^{\frac{1}{2}}$, whereas Equation (14) indicates a simpler form, $1/M$.

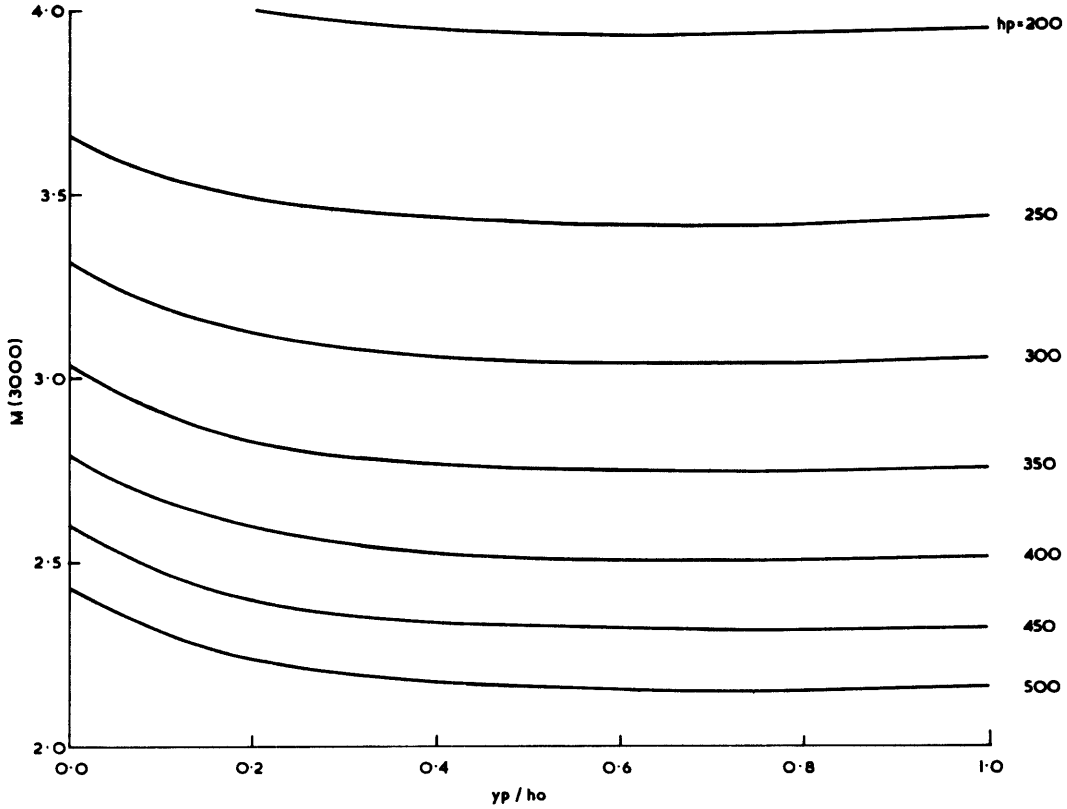

FIGURE 4

The $M(3000)$ factor as a function of yp/ho, parametric in hp. (After Appleton and Beynon, 1940.)

To test which form is better, the lines of best fit have been determined for a range of *yp/ho* between 0·0 and 1·0, for the following two cases:

(i) $$hp = a\frac{1}{M} - b, \tag{21}$$

(ii) $$hp = a'\frac{1}{(M^2-1)^{\frac{1}{2}}} - b', \tag{22}$$

where the slopes and intercepts are functions of *yp/ho*. The results of this analysis are shown in Table I.

TABLE I

	$hp = \frac{a}{M} - b$			$hp = \frac{a'}{(M^2-1)^{\frac{1}{2}}} - b'$		
yp/ho	*a*	*b*	σ	*a'*	*b'*	σ'
0·1	1601	199	3·8	1327	139	0·1
0·2	1513	182	3·4	1251	123	0·2
0·3	1490	180	3·8	1205	114	0·4
0·4	1439	167	3·8	1181	109	0·4
0·5	1428	165	3·5	1165	105	0·6
0·6	1425	165	3·2	1155	103	0·7
0·7	1437	170	3·4	1146	100	0·9
0·8	1420	163	4·0	1146	100	1·1
0·9	1415	161	3·3	1150	100	0·9
1·0	1422	163	3·0	1153	100	1·0
Median for *yp/ho* $\geqslant$0·4	1425	165	3·4	1153	100	0·9

This lists the slope, intercept and standard deviation (σ and σ' respectively) for each case. The uniformly small values of standard deviation indicate that both functions are good representations of the data. However, σ' is between 1 and 2 orders of magnitude smaller than σ, suggesting Equation (22) is the more precise formulation.

The results can be simplified to give valuable practical relationships as follows. Fig. 4 suggests that *hp* is almost independent of *yp/ho* when *yp/ho* $> 0{\cdot}3$. It is worthwhile, therefore, taking median values of the coefficients above this limit to give a single expression.
Thus

$$hp = \frac{1425}{M} - 165, \tag{23}$$

$$hp = \frac{1153}{(M^2-1)^{\frac{1}{2}}} - 100. \tag{24}$$

The usefulness of these equations can be assessed from a plot of the difference, Δ_1, between the median *hp* and that given by the general Equations (21) and (22) as a function of *yp/ho*. Fig. 5 gives the resulting variations of Δ_1, parametric in *M*, for the two formulations. For both, the following limit statements apply:

(i) $\Delta_1 \leqslant \pm$ 10 km. for $2 \leqslant M \leqslant 4$ and $1{\cdot}0 \geqslant yp/ho \geqslant 0{\cdot}38$,

(ii) $\Delta_1 \leqslant \pm$ 10 km. for $3 \leqslant M \leqslant 4$ and $1{\cdot}0 \geqslant yp/ho \geqslant 0{\cdot}22$.

These limits define the range over which Equations (23) and (24) adequately represent the family of Equations (21) and (22). In practice, for the *F2*-region, *yp/ho* and *M* almost always fall within limits (i) and (ii) so the median equations should be adequate for this region.

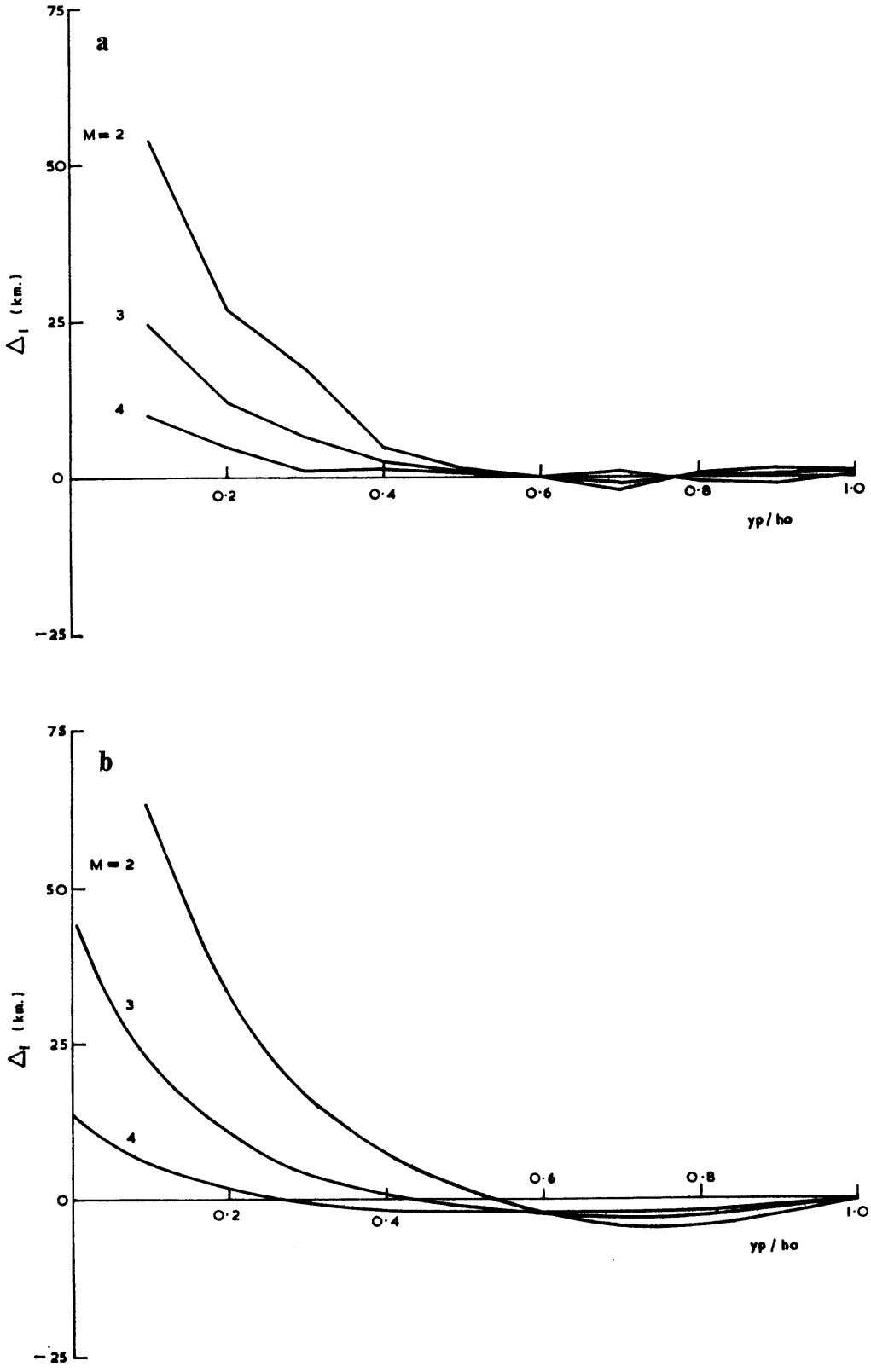

FIGURE 5

a. $\Delta_1 = hp$ (Equation 21)—hp (Equation 23) as a function of yp/ho, parametric in M.
b. $\Delta_1 = hp$ (Equation 22)—hp (Equation 24) as a function of yp/ho, parametric in M.
The noise in case (a) is consistent with the increased standard deviations in Table I.

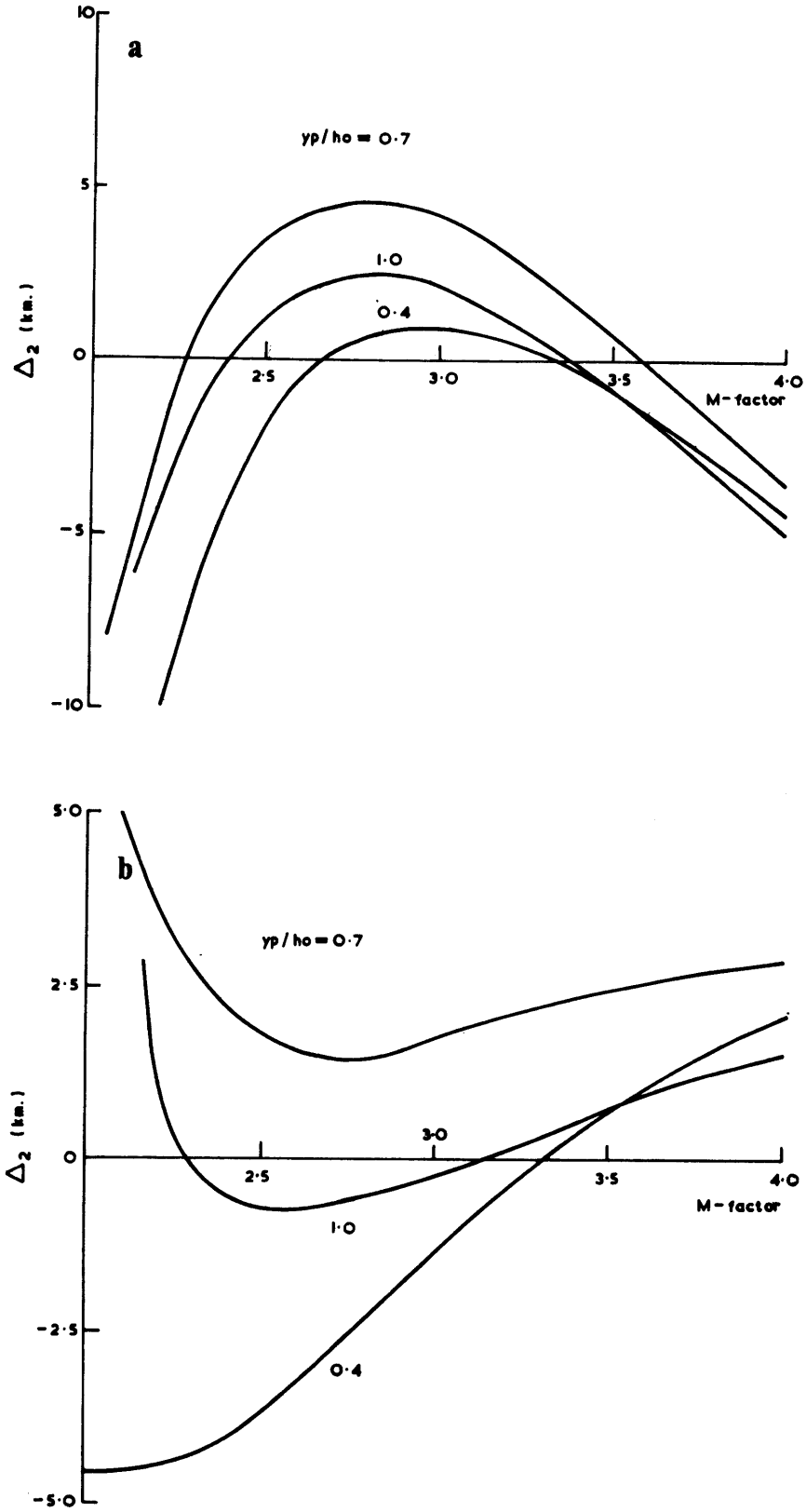

FIGURE 6

a. $\Delta_2 = hp$ (Equation 23)$-hp$ (actual), as a function of M, parametric in yp/ho.
b. $\Delta_2 = hp$ (Equation 24)$-hp$ (actual), as a function of M, parametric in yp/ho.

The degree to which the median equations represent the raw data (i.e. Fig. 4) is indicated in Fig. 6, where the difference between median and actual *hp*, Δ_2, is plotted as a function of *M*. As would be expected from the standard deviation results, Equation (24) is significantly better than Equation (23), though the latter is adequate for most applications.

5. *Shimazaki's derivation*

Appleton and Beynon's work showed that *hp* and *M(3000)* are related in a complex manner and the fact that simple forms of the type derived above (Equations (23) and (24)) existed was not realized for some years. It was not until 1955 that Shimazaki (1955) made the necessary simplifications in the theory to produce a simple explicit equation between *hpF2* and the *M*-factor, viz.

$$hpF2 = \frac{1490}{M} - 176. \tag{25}$$

Shimazaki demonstrated that this result was consistent with the direct methods of obtaining *hp* discussed on p. 5. The Shimazaki equation has been adopted by the international scientific community as the standard relationship. The new method of estimating *hmF2* described here is based on a similar approach. Shimazaki's derivation will therefore be discussed critically at this stage. But first a short digression into the background of one of Shimazaki's approximations is necessary.

Snell's law becomes invalid for a thick ionospheric layer, and Bouguer's rule must be employed. An exact treatment of the curved Earth case then requires integration along the path of the ray using a chosen $N(h)$ profile (i.e. Equation (19)). The difficulty of this procedure has caused some workers to search for simplifications such that μ at the point of reflection is given by

$$\mu_r = \sin i_0 G, \tag{26}$$

where *G* is a geometrical "fudge factor".

This approach relies essentially on the assumption that the path by which the ray reaches the reflection point is irrelevant, so that Bouguer's rule can be simplified by noting $i = 90°$ at reflection. Thus, referring to Fig. 7,

$$\mu_r = \frac{r_0 + ho}{r_0 + ho + z_0} \sin i_0,$$

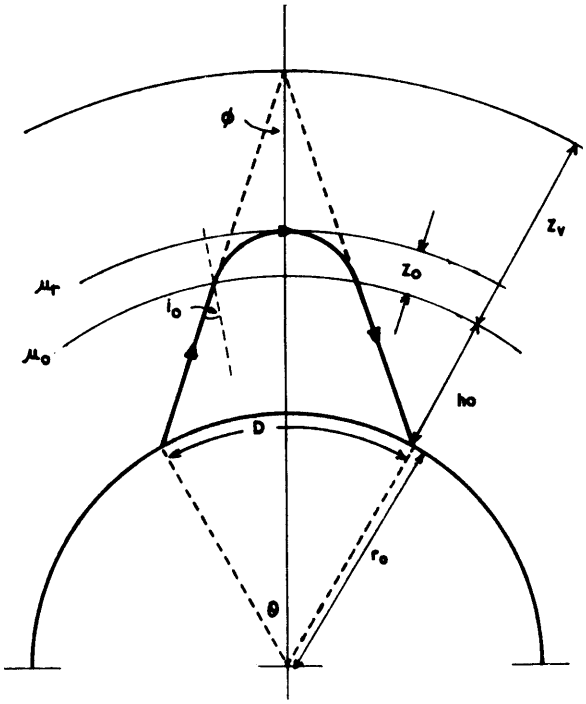

FIGURE 7
Construction for the Shimazaki (1955) derivation of *hp*.

from which

$$G = \left[1+\frac{z_0}{r_0+ho}\right]^{-1}. \tag{27}$$

Smith (1939) extended this approach by assuming N to be independent of h, giving μ = constant. This implies that generally

$$r \sin i = (r_0+ho) \sin i_0,$$

and in particular

$$(r_0+ho+z_0) \sin \Phi = (r_0+ho) \sin i_0 \tag{28}$$

from Fig. 7. It then follows by substituting Equations (27) and (28) in Equation (26) that

$$\mu_r = \sin \Phi \frac{1+z_v/(r_0+ho)}{1+z_0/(r_0+ho)}. \tag{29}$$

Shimazaki commenced his argument by quoting this result in the form

$$1+\left(\frac{f}{f'}\right)^2 = \sin^2 \Phi \left[\frac{1+z_v/(r_0+ho)}{1+z_0/(r_0+ho)}\right]^2,$$

where f' is the oblique path frequency and f the corresponding vertical incidence frequency. Shimazaki used the fact that z_0 and z_v-z_0 are both much less than r_0+ho to simplify this equation. The geometry of Fig. 7 was then used to eliminate Φ, giving

$$ho+z_v = -r_0\left(1-\cos\frac{D}{2r_0}\right)+r_0 \sin\frac{D}{2r_0}\left\{\left\{\frac{2(z_v-z_0)}{(r_0+ho)}\left(\frac{f'}{f}\right)^2+1\right\}/\left\{\left(\frac{f'}{f}\right)^2-1\right\}\right\}^{\frac{1}{2}}.$$

At this stage, Shimazaki made the major assumption that the Martyn equivalence theorem applied in the curved Earth case. This allowed the virtual height of reflection on the vertical path, h_v, to be equated with $ho+z_v$. Then assuming N varies parabolically with h and noting the Booker and Seaton (1940) result that $hp = h_v$ when $f = 0{\cdot}834fo$, it followed

$$hp = -r_0\left(1-\cos\frac{D}{2r_0}\right)+r_0 \sin\frac{D}{2r_0}\left\{\left\{2\left(\frac{z_v-z_0}{r_0+ho}\right)\left(\frac{f'}{f}\right)^2+0{\cdot}696\right\}/\left\{\left(\frac{f'}{f}\right)^2-0{\cdot}696\right\}\right\}^{\frac{1}{2}}.$$

The further assumption that $z_v = yp$ for $f = 0{\cdot}834fo$ gave $z_v-z_0 = 0{\cdot}55yp$. Taking r_0 = 6,370 km., D = 3,000 km. and ho = 200 km., the equation reduced to

$$hp = -176+1490\left\{\frac{0{\cdot}000168yp\,(f'/fo)^2+0{\cdot}696}{(f'/fo)^2-0{\cdot}696}\right\}^{\frac{1}{2}}. \tag{30}$$

Shimazaki realized that this equation applied for $f = 0{\cdot}834fo$ so that f' could not in general be the MUF. He showed, however, that it was related to the MUF such that

$$f' = foM(1+\zeta),$$

where

$$\zeta = \frac{\Delta f}{foM},$$

and $\Delta f = f'-MUF$. Thus the equation for hp could now be written

$$hp = 1490F(M, yp, \zeta)-176, \tag{31}$$

where

$$F(M, yp, \zeta) = \left\{\frac{0{\cdot}000168yp\,(1+\zeta)^2M^2+0{\cdot}696}{(1+\zeta)^2M^2-0{\cdot}696}\right\}^{\frac{1}{2}}. \tag{32}$$

Shimazaki found that the practical range of values for yp and ζ is limited. Data from Kokabunji gave mean values for these parameters of 90 km. and $-0{\cdot}05$, respectively, with a range of 5–10 per cent about these means. With these values, Equation (32) reduces to

$$F = \left\{\frac{0{\cdot}0196M^2+1}{1{\cdot}297M^2-1}\right\}^{\frac{1}{2}}.$$

For $2 \leqslant M \leqslant 4$, $1 \gg 0{\cdot}0196M^2$, so that

$$F \simeq \frac{1}{(1{\cdot}297M^2-1)^{\frac{1}{2}}}. \tag{33}$$

This approximation for function F results in an equation very similar in form to the $1/(M^2-1)^{\frac{1}{2}}$ result (Equation (24)). Noting $1{\cdot}297M^2 \gg 1$, F can be further simplified, giving

$$F \simeq \frac{1}{M}. \tag{34}$$

Shimazaki used this form for his final equation (Equation (25)) and demonstrated the validity of the approximation graphically by plotting $M.F$ as a function of M. Part of the resultant curve is reproduced in Fig. 8. It is apparent from this figure that the approximation holds to better than $\pm$ 1 per cent for $2{\cdot}1 \leqslant M \leqslant 3{\cdot}5$, and between -1 and $+4$ per cent for $2 \leqslant M \leqslant 4$.

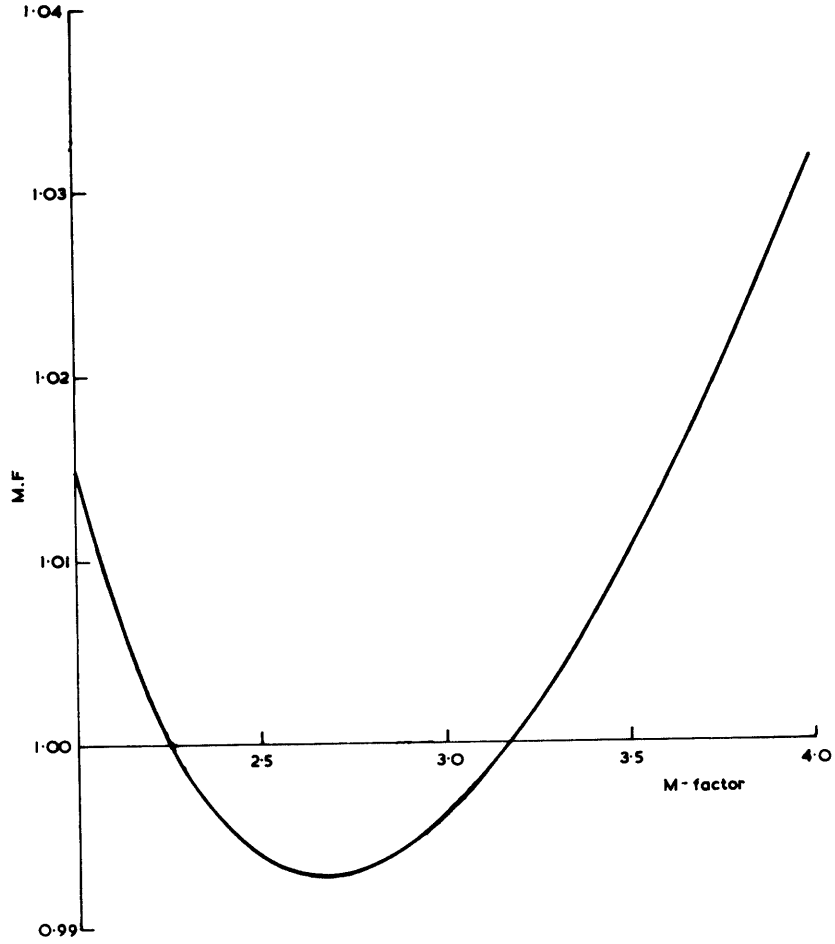

FIGURE 8

M.F (see Equation 32) as a function of *M*. Reproduction of part of the curve given by Shimazaki (1955) to justify his approximation for *F* (Equation 34).

Shimazaki showed that his final equation (Equation (25)) was relatively insensitive to changes in *yp* and ζ. This clearly must be so, because ζ is only a second-order term, whilst *yp* only figures in Equation (32) as part of a second-order term.

It may be assumed that the Appleton–Beynon analysis gives the precise solution for a simple parabolic layer, so that a comparison with this will highlight the effect of Shimazaki's approximations. The difference between Shimazaki's *hp* and the actual values (in Fig. 4) are shown in Fig. 9 as a function of *M* for $yp/ho = 0{\cdot}45$. This value of *yp*/*ho* is equivalent to Shimazaki's chosen values of *ho* and *yp*. In the figure, the dashed curve corresponds to the results using Equation (31), whilst the solid curve is for Equation (25).

The figure indicates that the approximation that Martyn's theorem holds, and the approximation that the path of the ray is irrelevant, together result in a more or less constant overestimate of between 10 and 15 km. Thus the shape of the function F is roughly correct but the coefficients of Equation (31) are not.

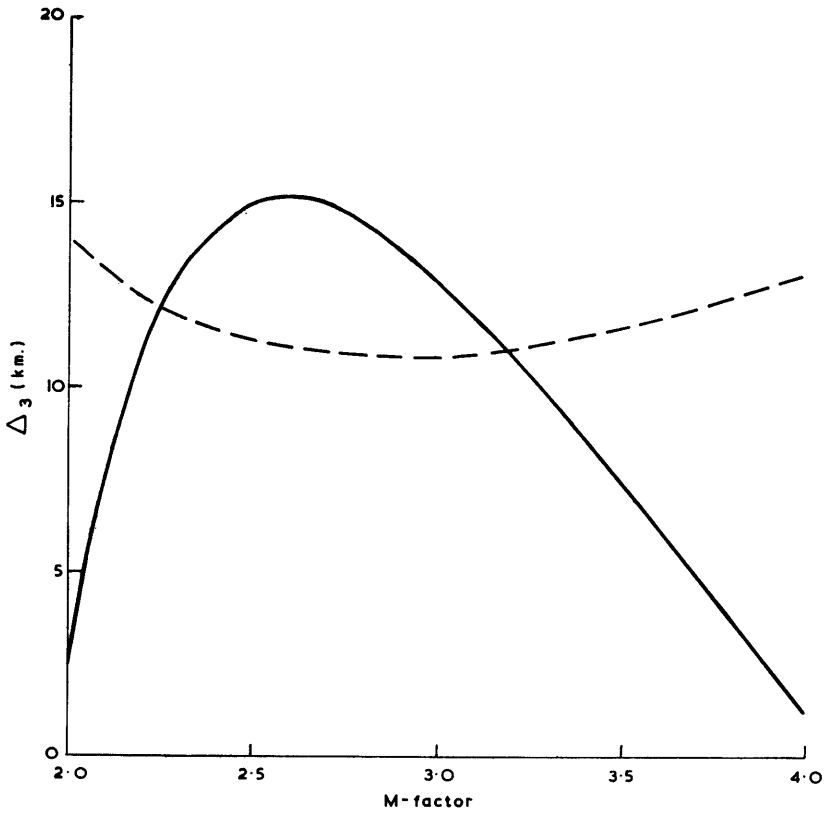

FIGURE 9

Comparison between the Shimazaki and Appleton and Beynon derivations of *hp*.
Dashed curve: $\Delta_3 = hp$ (Equation 31)—*hp* (actual).
Solid curve: $\Delta_3 = hp$ (Equation 25)—*hp* (actual).
The difference between the two curves indicates the distortion produced by the $1/M$ approximation.

As a corollary, the result of the simplifications is to reduce the effective *yp*/*ho* to about 0·2.

As might be expected from Fig. 8, the $1/M$ mathematical simplification introduces a distortion dependent upon M. This distortion is similar in form but of larger amplitude than that shown in Fig. 6a.

Considering the severity of the approximations, the discrepancies are remarkably small. This is the fortuitous result of cancellation of errors. The simple treatment of the ray path leads to an underestimate of the path length in the ionosphere, and hence the total range. This implies that for fixed D, the semi-angle Φ of the vertex of the equivalent triangle (Fig. 7) is overestimated. Consequently, from the geometry of Fig. 7, $ho+z_v$ will be underestimated. But, equating $ho+z_v$ with h_v by the equivalence theorem in the curved Earth case (personal communication from J. A. Murphy and P. A. Bradley) leads to an overestimate of h_v.

6. *Experimental evidence in favour of Shimazaki's equation*

It has been concluded that for a simple parabolic layer, in the absence of the B-field, the precise equations for *hpF2* as a function of *M(3000)F2* are found from Appleton–Beynon analysis, and that the Shimazaki equation produces a consistent overestimate. The experimental evidence appears to be at variance with this conclusion. Shimazaki, in his original paper, made comparisons between the values given by his equation using the measured *M(3000)F2* and those found by Booker and Seaton's method (see p. 5); these comparisons were made using data taken from observatories widely spaced over the globe. There does not appear to be any systematic trend in the differences between the two estimates of *hp*.

To resolve this inconsistency between theory and experiment, compare basic premises used in the two cases:

i. The parabolic approximation. Clearly the experiment and the theory are not compatible here. *M(3000)F2* and the Booker–Seaton *hp* were both determined from actual ionograms which contained varying amounts of underlying ionization. Both parameters would be affected by this. As will be seen later, the errors introduced would normally not be markedly different in the two cases. A special situation arises when the ratio of *foF2* to *foF1* is small enough for *hp* ($= 0{\cdot}834foF2$) to be measured at a frequency severely retarded by the *F1*-cusp.

ii. The effect of the *B*-field. It was demonstrated on p. 5 that the Booker–Seaton *hp* would be an overestimate of the true *hp* by an amount depending upon the magnetic dip at the location in question. The effect of the *B*-field is not included in the calculations used to construct *MUF* overlays so it is possible that the value of *M(3000)F2* determined for a particular *hp* will vary with dip. This introduces a source of inconsistency into the experimental comparison, but it is possible to test the effects produced, as will be seen below.

iii. The method of measuring *M(3000)F2*. This is the critical point and is discussed at length. For the simple case of flat Earth, flat ionosphere and no magnetic field, the equivalence theorem linking the vertical and corresponding obliquely propagated ray (see Fig. 3a) leads to the simple equations

$$f = f_v \sec i_0,$$
$$D = 2h' \tan i_0.$$

Smith (1937) proposed a graphical solution of these equations for application to ionograms with logarithmic frequency scales. A curve is constructed with h' as ordinate (on the same scale as the ionogram height scale) and sec i_0 as abscissa (plotted on a logarithmic scale in the reverse direction to the ionogram frequency scale). Obviously, a family of curves can be drawn, each for a different ground range D. By overlaying the curve (called a *transmission curve*) on the ionogram and moving it, maintaining a match between the two height scales, until the $h'f$ curve and transmission curve just touch, the maximum usable frequency factor for the range D can be determined. The value is simply given by the cutting point on the sec i_0 scale corresponding to the critical frequency on the ionogram. For the special case considered the solution is exact.

The solution of the general case of curved Earth and curved ionosphere depends on the actual electron distribution encountered by the ray. As already discussed, Appleton and Beynon solved the problem completely for the case of a parabolic distribution, and in a subsequent paper (Appleton and Beynon, 1947) they gave computed values of the *MUF* factor in the overlay form discussed above. Because, in their theory, the *MUF* factor is a function of *yp*/*ho*, the values were stated for the average variation of this parameter with height over Slough. Smith (1937, 1939) also tackled the general problem; in his approach it was assumed initially that the Earth was curved whilst the ionosphere was flat. This allowed the factors to be determined approximately without reference to the actual ionization distribution. The values thus obtained were then modified by an approximate correction factor derived by assuming a linear electron distribution.

The values of M as a function of h' (required to make an *M(3000)F2* slider) deduced by Smith differ slightly from those obtained by Appleton and Beynon and, of course, neither precisely describes conditions in the real ionosphere. Notwithstanding this, it was agreed internationally that Smith's values should be taken as standard. For the present purpose, the significant point is that Shimazaki used Smith-type approximations in his derivation. The international factors are thus more consistent when used in Shimazaki's equation than the Appleton–Beynon analysis. Conversely, Appleton–Beynon factors used in Shimazaki's equation will produce worse results than the international factors.

The points raised in (ii) and (iii) can be tested using Becker's (1960) tables giving $h'f$ curves for parabolic layers in the presence of the *B*-field. Table II shows the results of such a test in which the values of *M(3000)F2* were determined from these $h'f$ curves, first using the international slider and then the Appleton–Beynon slider. The semi-thickness of the model layer was fixed at 100 km. and *hp* was varied between 200 and 400 km. The tests were made for two very different values of dip and in each case the value of *hp* given by Shimazaki's simple equation and the value from the Booker–Seaton method were determined. The table demonstrates the following points:

TABLE II
COMPARISON OF DIFFERENT METHODS OF EVALUATING *hp*

True value of hp	*200*	*250*	*300*	*350*	*400*	
hp from Shimazaki equation using the international factors	216	262	305	347	386	
hp from Shimazaki equation using the *A*/*B* factors	216	269	316	362	397	Dip = 10°
hp by Booker and Seaton's method (*h'* at 0·834*foF2*)	203	253	303	353	403	
hp from Shimazaki equation using the international factors	229	276	321	366	397	
hp from Shimazaki using the *A*/*B* factors	228	282	333	376	420	Dip = 60°
hp by Booker and Seaton's method	213	263	313	363	413	

i. For both dips the international factor gives a better value of *hp* than does the *A*/*B* factor, except at the lowest and greatest heights. The corollary to this is that the international factors will give less precise values for *hp* when used in the *A*/*B* equations than they will in the Shimazaki equation.
ii. As the dip increases, calculated *hp* increases (for constant true *hp*), because *M*(3000)*F2* decreases. This is in the same sense as the magnetic field effect in the Booker–Seaton *hp*. Note that the values obtained from the international factors and those obtained from Booker–Seaton remain internally consistent as dip increases.

It is now clear why the Shimazaki equation gave good agreement with the Booker–Seaton *hp*. The errors in this equation are compensated to some extent by similar errors in the analysis for the *MUF* factor. Both methods of estimating *hp* overestimate by similar amounts because of the effects of the *B*-field.

Obviously, Becker's tables could be used to establish accurate relationships between *hp* and *M*(3000)*F2* (using the international factors), parametric in magnetic dip. A preliminary analysis suggests that the $1/(M^2-1)^{\frac{1}{2}}$ formulation is better than the $1/M$ and that the coefficients a' and b' both increase with increasing dip.

7. *Summary*

The basis for a simple relationship between the *M*(3000)*F2* factor and *hpF2* has been discussed. It has been shown that, whilst the approximations used by Shimazaki in his derivation result in an equation which is fundamentally inaccurate, similar inaccuracies in the accepted method for determining *M*(3000)*F2* tend to compensate. The Appleton–Beynon analysis is inherently more exact but cannot be of practical use because of the bias in the international factors. However, it is clear that the $1/(M^2-1)^{\frac{1}{2}}$ formulation is preferable to the $1/M$ approach. It has been noted that Shimazaki's use of $1/M$ introduces significant distortions when compared with his more complete equation. A method by which more accurate relationships between the international factor and *hpF2* could be derived, including the effect of the geomagnetic field, has been suggested.

The aim of the work described in this report is the development of a simple empirical equation for *hmF2*. As a first step, therefore, the recognized form of Shimazaki's equation will be used but the insight gained from the analysis in this section will be utilized to locate where and how the resultant expressions break down.

III. CORRECTION FOR THE EFFECTS OF UNDERLYING IONIZATION

1. *Introduction*

It was quickly realized that *hp* could not be simply equated with *hm* except under very special conditions. These were:

i. That the layer in question was parabolic in form at all heights.
ii. That the group retardation suffered by radio waves (at the sampling frequencies) traversing underlying layers or non-parabolic parts of the reflecting layer was negligible.

For the *F2*-layer these conditions only occur at night during magnetically quiet conditions. At other times condition (i) is usually a reasonable approximation, but condition (ii) is certainly not, and the use of *hp* will lead to overestimates of *hm*, often by more than 50 km.

In this section some basic ideas concerning the effects of underlying ionization are illustrated. This is followed by a critical review of previous work on model methods of estimating *hmF2* and *ymF2*.

2. *Basic ideas*

The effects of underlying ionization are best understood by considering the group retardation suffered by a wave (frequency f) due to a simple model layer of critical frequency fo, where $f \geqslant fo$. Three different cases are considered but the effect of the *B*-field and energy loss due to collisions are neglected.

i. The electron concentration (N) does not vary with height (slab). In this case the group retardation expressed as the difference between the true and virtual heights normalized by the layer thickness (ym) is

$$\frac{\Delta h'}{ym} = \left[1-\frac{1}{x^2}\right]^{-\frac{1}{2}}-1, \tag{35}$$

where $x = f/fo$.

It is a simple matter to show that the total electron content, $\int N\mathrm{d}h$, of this layer is $ymNo$.

ii. N parabolic with height (up to hm)

$$\frac{\Delta h'}{ym} = x \operatorname{arc\,tanh} \frac{1}{x}-1, \tag{36}$$

$$\int N\mathrm{d}h = \frac{2}{3}ymNo.$$

iii. N linear with height

$$\frac{\Delta h'}{ym} = 2x^2\left\{1-\left[1-\frac{1}{x^2}\right]^{\frac{1}{2}}\right\}-1, \tag{37}$$

$$\int N\mathrm{d}h = \frac{1}{2}ymNo.$$

These normalized group retardations are given in Fig. 10 as functions of x for $1 \leqslant x \leqslant 2$. Also shown

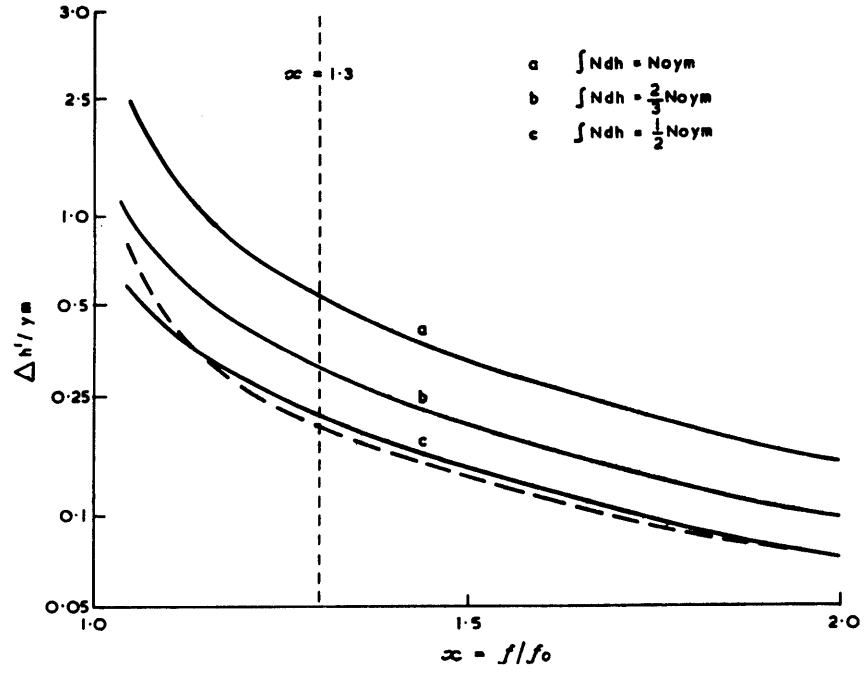

FIGURE 10

Normalized group retardation suffered by a wave of frequency f in penetrating a layer of critical frequency fo ($f>fo$).
a. For a slab. b. For a parabola. c. For a linear layer.
The dashed line shows the corresponding curve for the parabola when the magnetic field is included.

in the figure is the corresponding curve for a parabolic distribution when the *B*-field is included (taken from Becker (1960) for $I = 60{\cdot}0°$). The no-field curves have, to a first approximation, the same shape above a limit value of x of about $1{\cdot}3$; the differences between them above this limit are almost entirely due to the changes in $\int N dh$. Thus, the shape of the underlying profile is immaterial for group retardation on frequencies above this limit and only the underlying total content matters. This is a crucial point because it means that any convenient model profile can be used to correct *hp* provided the total content is approximately right. Also, minor perturbations in the real profile shape (for example, the appearance of an *F1*-cusp) are unimportant provided x is above the limit value. This point has also been made by Lawrence and others (1964) in a discussion of ionospheric perturbations on V.H.F. signals.

A further advantage is found in practice because the *B*-field moves the critical point much closer to the cusp (x of the order of $1{\cdot}05$; the dashed curve in Fig. 10). It is noteworthy, also, that the no-field linear distribution, which has the great advantage of mathematical simplicity, is a very good approximation of the full-field parabolic case for $x > 1{\cdot}05$.

It is unusual for $x < 1{\cdot}05$ to occur in practice, so the comment made on p. 17 concerning the effects of underlying ionization on *hp* and *M(3000)F2* is seen to be true. In the extreme case, both will be greatly affected but to differing degrees because the measuring point for *hp* is at a lower frequency ratio than is the tangency point for *M(3000)F2*.

3. *Review*

Booker and Seaton (1940) were among the first workers to realize the need for a simple method of correcting *hpF2* for underlying ionization. They developed a method in which the *F2*-layer and both the underlying layers (*E*, *F1*) were approximated by parabolic ionization distributions (see the example in Fig. 11). Estimates of the height and semi-thickness of the *E*-layer were made using the technique discussed

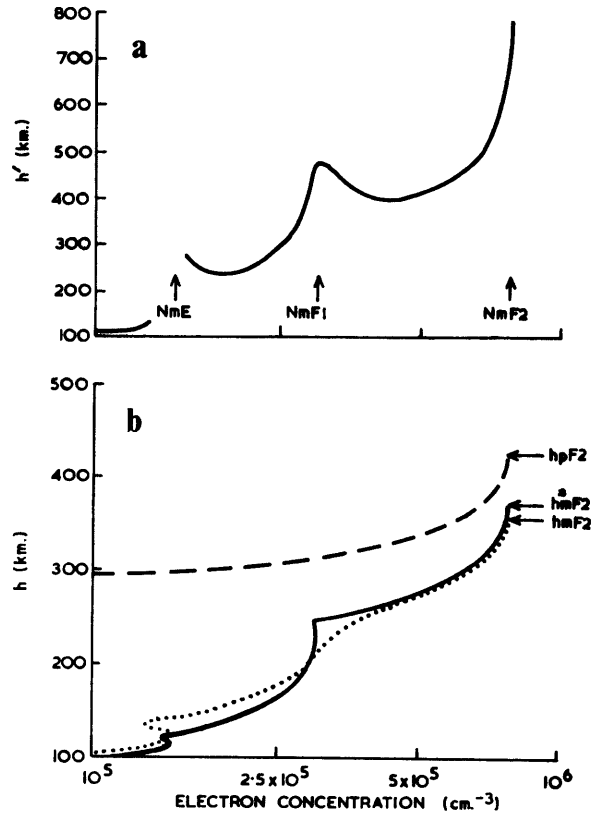

FIGURE 11

Practical example of the "Booker–Seaton" correction technique. Shown in the figure are: a. The ordinary trace in terms of N recorded at the Argentine Islands on 31 December 1967 at 13.30 L.T. b. Dashed curve: the simple parabola obtained if no correction for underlying ionization is made; solid curve: the "Booker–Seaton" triple parabola construction; dotted curve: $N(h)$ profile deduced from ionogram using a sophisticated numerical method.

on p. 5. Given these, the virtual heights required to determine the corresponding parameters for the *F1*-layer were corrected for group retardation in the *E*-layer, using Equation (11). This procedure was then repeated to give, finally, estimates of *hmF2* and *ymF2* (call them $\hat{hm}F2$ and $\hat{ym}F2$ to differentiate them from the true values).

For the example shown, the Booker–Seaton correction scheme produces a good estimate of *hmF2* since the parabolic profile has about the same underlying total content as the actual profile. However, the layer-like properties of the *F1*-region are seen to be considerably accentuated. The method is not practical since each determination of $\hat{hm}F2$ requires considerable analysis of the original ionogram. The Booker–Seaton approach is historically important because it introduced the idea of the triple-parabola approximation, much used in subsequent analyses. Ratcliffe (1951) developed the Booker–Seaton analysis into a graphical technique. This method has the advantage of speed but is relatively inaccurate.

Vickers (1959) attempted to derive a more practical scheme for correcting *hpF2* by making the assumption that only the *F1*-layer made a significant contribution to the group retardation near *hp*. This is clearly a reasonable approach because $\int N\mathrm{d}h$ is much smaller for the *E*-region than for the *F1*. Vickers used a model profile for the underlying layer and derived expressions of the form of Equations (35) to (37), where $x'_F = foF1/foF2$. The model profile results were calibrated using observational data ($N(h)$ profiles deduced from Slough ionograms) and Vickers found that the slab (Equation (35)) gave the best results. His estimate of *hmF2* was therefore

$$\hat{hm}F2 = hpF2 - a\left[(1-x'^2_F)^{-\frac{1}{2}} - 1\right] - b, \tag{38}$$

where a and b are numerical coefficients obtained by linear regression analysis of the sample data (Vickers obtained a correlation coefficient of 0·88). "a" is a function of the mean value of *ymF1* in the sample used. "b" should ideally be zero, but in Vickers' analysis was negative for low sunspot numbers and positive at high sunspot numbers.

The Vickers method allows a crude approximation to be made for a particular location once the calibration has been made. It has the advantage over Booker–Seaton's correction scheme in that it relies only upon published data; there are, however, two important criticisms:

i. A correction can only be made when a scaleable *F1* critical frequency is present on the original ionogram. An *F1*-critical is usually produced by an inflexion in the $N(h)$ profile and not a turning point (see Fig. 11). A small change in the shape of the profile near 200 km. can therefore cause the "*F1*-layer" on an ionogram to disappear without greatly changing the group retardation produced on a higher frequency. The result would be a serious overestimate of height.

ii. The coefficients a and b are strongly dependent on sunspot number, and extra analysis would be required to establish the form of this and the resulting empirical equations would be unnecessarily complex.

Wright and McDuffie (1960) made an empirical analysis of the validity of *hpF2* as an estimate of *hmF2* using sunspot-maximum $N(h)$ profile data and corresponding values of *M(3000)F2* from 16 observatories covering a wide latitude range. They found that the approximation was valid at night-time at low and middle latitudes, but not at high latitudes where $\hat{hm}F2$ was always less than *hpF2*. During the daylight hours *hpF2* was an overestimate at all latitudes. However, at low and middle latitudes the relationship between *hm* and $1/M$ was still substantially linear so Wright and McDuffie proposed the new empirical relation

$$\hat{hm}F2 = \frac{1411}{M} - 169. \tag{39}$$

This equation was found to be inadequate at high latitudes during the day.

The practical value of Equation (39) is limited because variations in the amount of total underlying ionization have been smoothed out.

A graphical method of obtaining $\hat{hm}F2$ and $\hat{ym}F2$ has been developed by Taieb (1967). He assumed a parabolic layer approximation but took account of the Earth's magnetic field. Taieb tried to devise a scheme which would require only parameters routinely scaled from ionograms, but he found it necessary to introduce a new parameter: the frequency at which the lowest virtual height is recorded from the *F2*-region. Thus, the usefulness of his method is greatly reduced.

Decker (1972) has developed a method which relies only on the routinely scaled parameters *foE*, *foF2*, *M(3000)F2* and *h'F*. He assumed a model ionosphere composed of two α-Chapman type layers, an *E* and an *F2*; *hmE* is taken as fixed at 108·6 km. and *HE* (the scale height of the *E*-layer) as 7·5 km. From this model, Decker has calculated *M(3000)F2* for a range of $h\overset{*}{m}F2$, *HF2* (scale height of *F2*-layer) and x'_E ($=foE/foF2$). A polynomial three-dimensional fit to the resultant matrix of points gives the equation

$$h\overset{*}{m}F2 = \sum_{r=0}^{3}\sum_{q=0}^{3}\sum_{p=1}^{4} x'^{r}_{E}\left(\frac{1}{M}\right)^{q}(HF2)^{p-1}(DK)_{p+q+r}.$$

In this equation, $(DK)_{p+q+r}$ represent 64 coefficients produced by the fitting process. Before $h\overset{*}{m}F2$ can be determined *HF2* must be known; Decker showed that this could be represented by

$$HF2 = \sum_{r=0}^{4}\sum_{q=0}^{3}\sum_{p=1}^{3} x'^{r}_{E}\left(\frac{1}{M}\right)^{q}(h'F)^{p-1}(BK)_{p+q+r}.$$

These two remarkable equations correct for the relatively small effect of the *E*-region whilst entirely ignoring the major contribution of the ionization between the *E* and *F2* layers. Decker pointed out that the inclusion of this would necessitate a five-dimensional polynomial. Not surprisingly, the computer available to Decker could not cope with this, but he was able to obtain an approximate result by assuming $h\overset{*}{m}F1 = 210$ km., $HF1 = 21$ km. and $foF1 = 1{\cdot}4foE$.

Decker's method cannot be considered as practical because it is extremely cumbersome and does not correct for the major term (the coefficients required in the special three-layer solution are not quoted).

Bradley and Dudeney (1973) made quite a different approach to the problem. They realized the crucial point that only the total underlying content was important. They found that the simplest way to treat the problem was to use a model consisting of a parabolic *E*-layer, a parabolic *F2*-layer, and a linear increase in electron concentration fitting the profile between these two and chosen to give the required total content (see Fig. 12). *hmE* was fixed at 110 km. and *ymE* at 20 km. By trial and error, it was found that the best agreement with *N(h)* analysis was obtained when the electron concentration at which the linear portion intersected the *F2*-parabola equalled $2{\cdot}89NmE$ ($1{\cdot}7foE$). A particular feature of the model is that ionization in the *F1* height range is determined by *E* and *F2* ionization parameters. Bradley and Dudeney pointed out that measured true-height profiles rarely show marked *F1*-layer discontinuities; many of the cusps and inflexions seen on ionograms which are scaled as *F1*-layer characteristics result from only minor fluctuations in electron concentration (see Fig. 11). They stressed that it is the ionization between the *E* and *F2* regions which contributes most to the group retardation at *hpF2*, and that this is present irrespective of the behaviour of the *F1*-ledge.

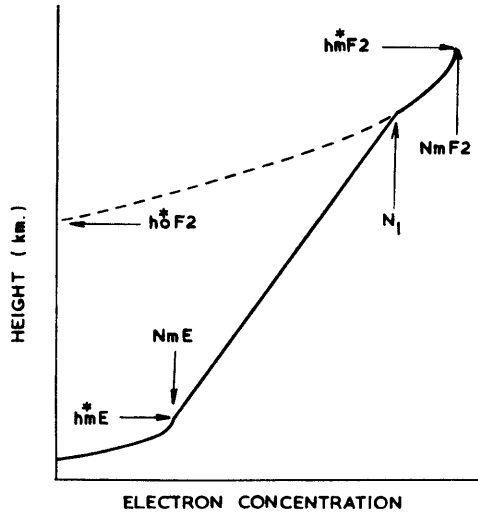

FIGURE 12

The simplified *N(h)* profile used by Bradley and Dudeney (1973).

Bradley and Dudeney synthesized ionograms, neglecting the *B*-field, for a wide range of values of the parameters $h\dot{m}F2$, $y\dot{m}F2/h\dot{o}F2$ and x_E ($=foF2/foE$). *M(3000)F2* was measured on these ionograms using the standard international procedure (Piggott and Rawer, 1972). This parameter was found to be relatively insensitive to $y\dot{m}F2/h\dot{o}F2$ and the results were consistent with the following empirical relations which apply for $x_E > 1{\cdot}7$.

$$h\dot{m}F2 = a(M)^b$$

$$\left.\begin{aligned} a &= 1890 - \frac{355}{x_E - 1{\cdot}4} \\ b &= (2{\cdot}5x_E - 3)^{-2{\cdot}35} - 1{\cdot}6 \end{aligned}\right\} \tag{40}$$

$$\left.\begin{aligned} y\dot{m}F2 &= h\dot{m}F2 - (h'F\,(F2) - \Delta h') \\ \Delta h' &= \left[\frac{0{\cdot}613}{x_E - 1{\cdot}33}\right]^{0{\cdot}86} (h\dot{m}F2 - 104). \end{aligned}\right\} \tag{41}$$

$h'F(F2)$ is the minimum observed virtual height of reflection from the *F2*-layer; it is equal to $h'F$ in the absence of an *F1*-ledge and $h'F2$ at all other times. The reason for the limit value $x_E = 1{\cdot}7$ is obvious and it is of note that this implies a value of about $1{\cdot}2$ for x_F ($=foF2/foF1$), well above the limit at which the shape of the underlying profile becomes important in practice (Fig. 10, field case).

Bradley and Dudeney compared the values obtained from Equations (40) and (41) with values determined by *N(h)* analysis using ionograms from a number of different locations. This comparison was made using data from all seasons and from both extremes of the solar cycle. The agreement was generally very good, and in particular the claim that the presence or absence of the *F1*-ridge has insignificant effect on the group retardation was supported by the comparison results.

Bradley and Dudeney have undoubtedly developed a very powerful method of estimating *hmF2* and *ymF2* which should find wide application in morphological studies of the *F*-region. For the present purposes, however, the limitation that the method cannot be used when x_E is less than $1{\cdot}7$ can be important, since such values of x_E are often found at middle and high latitudes during the daytime in summer. Also, it is desirable to allow for the effects of the *B*-field.

4. *Summary*

To obtain a true value of *hmF2* on all occasions would involve making a precise *N(h)* computation from the actual ionogram which is a slow and expensive procedure.

To avoid this expense, various authors have attempted to estimate *hmF2* by using idealized models of the ionosphere. This has been done using either a general model applicable over wide areas (i.e. Bradley and Dudeney) or by a model selected and calibrated to fit the ionosphere at a particular location (e.g. Vickers). Provided a suitable choice of parameters is made, coupled with careful analysis of sample data, the latter method is capable of higher accuracy than the former for studies at one station. A "data calibration" type of approach has therefore been selected in the method described below.

IV. ANALYSIS

1. *Introduction*

In this section, a method for estimating the true height of the *F2*-layer is described in which Shimazaki's equation is used but a correction for underlying ionization is made. Following the work of Bradley and Dudeney (1973), it is assumed that the correction term can be expressed as a function of x_E alone, independent of the behaviour of the *F1*-ledge. The form of the function is determined empirically using true-height data for the location in question.

The standard form used by many authors in the past for correcting *hpF2* for the effects of underlying ionization is

$$h\dot{m}F2 = hpF2 - \Delta h, \tag{42}$$

where Δh is a height-correction term expressed as some known function of the total underlying ionization. The form of this function can be found either by explicit use of a model profile or by using the Vickers type approach. For simplicity it is usually taken as parametric in x, where x is the ratio of the maximum plasma frequency of the underlying ionization to *foF2*. In its general form, the "Δh" correction method is quite valid but difficulties arise in practice when the total underlying ionization is assumed to be given by a function of x alone. The total underlying ionization can change with *hmF2*, causing the required Δh to increase with increasing *hmF2* except in the unlikely case where the layers are completely separated. A simple type of variation with x can be obtained only if Δh is normalized by the thickness of the underlying layer (see the work of Vickers, p. 21). However, another unknown variable is thereby introduced.

In this analysis an entirely different approach is adopted which automatically allows for changes in *hmF2* without requiring a value for the underlying layer thickness. Consider the Shimazaki equation.

$$hpF2 = \frac{1490}{M_0} - 176,$$

where the subscript "$_0$" denotes an observed value. Differentiating and approximating to small finite changes gives

$$\Delta h \simeq \frac{1490 \Delta M}{M_0^2}. \tag{43}$$

If Δh is the value which satisfies Equation (42), ΔM can be taken as the increment to M_0 required in the Shimazaki equation to give $\dot{hm}F2$, viz.

$$\dot{hm}F2 = \frac{1490}{M_0 + \Delta M} - 176. \tag{44}$$

It is reasonable to suppose that ΔM can be expressed approximately by a function $\phi_M(x_E)$, thus at constant x_E, ΔM is constant and it is clear from Equation (43) that Δh is an inverse function of M_0 and hence some direct function of *hmF2*. There are therefore marked practical advantages in using ΔM instead of Δh for estimating $\dot{hm}F2$. This will be called the "ΔM" approach.

This section is devoted to establishing empirically the form of the function $\phi_M(x_E)$ to be used in Equation (44). As part of this analysis the "ΔM" method will be tested against the "Δh" method experimentally. It will be shown that by using the "ΔM" approach a single equation for $\dot{hm}F2$ can be obtained which is applicable at all epochs of the solar cycle, an important practical point.

2. *The data sample*

The objectives of the data analysis have been defined and it is now necessary to consider the practical details involved in some depth. A set of data is required comprising of values of $\dot{hm}F2$ (obtained by numerical $N(h)$ analysis) with the corresponding $M(3000)F2$'s and x_E's. This set must be complete enough to describe the behaviour of the layer both diurnally, seasonally and at different solar epochs. However, the total number of determinations of $\dot{hm}F2$ that can reasonably be made depends upon the time taken over each determination. This time is controlled by the type of $N(h)$ analysis used. Since the study is manpower limited, the fastest method available (commensurate with maintaining adequate accuracy) must be employed to maximize the data set. It should be noted that a full $N(h)$ profile is not required, only $\dot{hm}F2$. Bearing these points in mind, the "*hcqc*" method (Piggott and Rawer, 1972) will be used.

In this technique, the true height (h_3) at a plasma frequency (f_3) equal to 0·95 of the critical frequency *foF2* is determined using the "10-point" method (Schmerling, 1958, 1967). The latter is a simple numerical method designed specifically for manual use, which includes correction for the effects of the geomagnetic field, and in which the only assumption made about the profile is that it be monotonic. The quarter thickness (qc) of the equivalent parabolic layer which matches the $N(h)$ profile above f_3 is determined directly from the ionogram by an overlay technique. The true height of the peak (*hcF2*, for this method) is given by $hcF2 = h_3 + 0{\cdot}625qc$. Each determination of *hcF2* takes between 5 and 10 min., depending on the type of ionogram (those with logarithmic scales are more convenient), whereas a computer-based system (for finding the $N(h)$ profile and thereby $\dot{hm}F2$) will in practice be between 10 and 100 times slower.

To understand the mechanics of Schmerling's 10-point method, consider again Equation (6)

$$h'(f) = \int_0^f \mu' \frac{dh}{df_N} df_N + h(o);$$

for a particular value of f_N this equation can be inverted (Budden, 1955) to give

$$h(f_N) = A_{N1}h'(f_1) + \ldots A_{NS}h'(f_S) + \ldots A_{NN}h'(f_N).$$

Here $h'(f_S)$ is the virtual height at a plasma frequency f_S, less than or equal to f_N, and the coefficients A_{NS} are all different. Not only do these coefficients vary with f_S but also with f_N and different sets are needed for different geomagnetic locations. Schmerling showed, however, that values of the ratio f_S/f_N could be found such that all the coefficients were equal; h was then simply the sum of the h' values divided by the number in the sample. Furthermore, the sampling ratios (f_S/f_N) were found to be only slowly varying functions of both frequency and the magnetic parameters so that one set could be used for a moderate range of values. Schmerling chose ten sampling frequencies so that

$$h = \frac{1}{10}\sum_{1}^{10}(h_i').$$

The accuracy of the "*hcqc*" method depends intimately upon the type and quality of the ionogram to which it is applied. The ionosonde in operation at the Argentine Islands is a Union Radio Mark II type which produces an ionogram with a non-logarithmic frequency scale from which heights may normally be scaled to $\pm 5{\cdot}0$ km. and frequencies from $\pm 0{\cdot}02$ to $\pm 0{\cdot}05$ MHz (as a function of frequency). Restricting the discussion to this type of ionogram,

$$h_3 = \frac{1}{10}\sum_{1}^{10}(h_i').$$

If the uncertainty in the i^{th} value of h' is $\delta h'_i$, the maximum uncertainty can be represented by

$$\delta h_3 = \pm \sum_{1}^{10}\left(\frac{\partial h_3}{\partial h'_i}\right)\delta h'_i$$

or

$$\delta h_3 = \pm \frac{1}{10}\sum_{1}^{10}(\delta h'_i). \tag{45}$$

The most probable error in h_3, Q_3, is given by

$$Q_3 = \pm \left\{\sum_{1}^{10}\left[\left(\frac{\partial h_3}{\partial h'_i}\right)\delta h'_i\right]^2\right\}^{\frac{1}{2}},$$

therefore

$$Q_3 = \pm \frac{1}{10}\left\{\sum_{1}^{10}(\delta h_i)^2\right\}^{\frac{1}{2}}. \tag{46}$$

For a perfect ionogram, the quoted frequency uncertainties will introduce no significant height uncertainty and $\delta h'$ will equal ± 5 km. for all i. It follows from Equation (45) that $\delta h_3 = \pm 5$ km. also; further, from Equation (46) $Q_3 = \pm$ 2 km. In practice, one or more of the h'_i values may have to be estimated either because the sampling point falls on a cusp, or because the relevant part of the trace is missing. Provided the number of such cases is small, the resultant measuring uncertainty will only be marginally increased as individual errors carry one-tenth weight in the average.

Piggott (1954) pointed out a further possible source of error in sampling methods such as Schmerling's. The true heights determined in the vicinity of cusps tend to be slightly high and those away from cusps correspondingly low, such that the total area under the resultant $N(h)$ curve remains approximately correct. The Schmerling method may therefore slightly underestimate h_3.

The accuracy of *hcF2* also depends upon the measurement of *qc*. Using the overlay technique described by Piggott and Rawer (1972) for non-logarithmic ionograms, the best measuring accuracy obtainable in *qc* is ± 5 km. Operationally, the maximum uncertainty is probably of the order of ± 10 km. and there may be additional unknown errors if the real profile departs significantly from the parabolic form above $0{\cdot}95 foF2$. Taking δqc as ± 10 km. the maximum uncertainty in *hc*, δhc, is given by $\delta h_3 + 0{\cdot}625\delta qc$, i.e. approximately

11 km. The most probable uncertainty in this parameter is approximately 7 km. Allowing for systematic effects in the 10-point method and for non-perfect ionograms, the probable uncertainty in *hc* is increased to about ± 10 km., independent of *hc*.

As a test of consistency, four ionograms were reduced, both using the methods just discussed, and a sophisticated numerical method developed by Jackson (1971). He included the effects of the Earth's magnetic field and also included an estimation of the depth of the valley above the *E*-layer. The latter calculation is performed by varying the chosen depth of the valley until the observed and computed extraordinary traces match. The Jackson system involves a parabolic extrapolation to the peak of the layer based on the values of N, h and $\partial N/\partial h$ determined at the last two points scaled from the ionogram. From this extrapolation estimates of *hmF2*, *ymF2* and *NmF2* are obtained.

The values found from the four ionograms are given in Table III, in which *foF2* is the observed value

TABLE III

COMPARISON OF MANUAL AND COMPUTER METHODS FOR ESTIMATING *hmF2*

"*hcqc*"				"*Jackson*"			
h_3	*hc*	*qc*	*foF2*	h_3	$\dot{hm}$	$\dot{qm}$	$\dot{foF2}$
319	363	70	7·90	317	358	60	7·89
324	361	60	11·25	324	359	53	11·32
270	301	50	6·00	279	315	51	6·02
241	263	35	8·25	244	278	48	8·38

and $\dot{foF2}$ is the value calculated by parabolic extrapolation. In the Jackson case h_3 was determined by using the observed value of *foF2*. It will be noted that in three out of the four cases the h_3's agree to within $\pm$ 3 km., suggesting that both methods are capable of producing quite accurate answers for this parameter. However, the agreement is less exact for the parameters determined using the two different parabolic extrapolations.

These discrepancies highlight an important point often overlooked by workers involved in $N(h)$ analysis. Numerical methods of extrapolation, of which Jackson's is but one, rely upon two measurements of h' at a sensitive part of the $h'(f)$ profile (near *foF2*) where small errors in the measurement of frequency produce disproportionate errors in true height. Because of this, such methods cannot be expected to give precise values of $\dot{hm}$ and $\dot{ym}$, although the errors can be reduced by repeating the procedure and averaging the results. On the other hand, in the "*hcqc*" method, the shape of the observed $h'(f)$ profile above $0{\cdot}95foF2$ is matched by eye with one of a family of standard shapes, giving an inherently more exact result. The Jackson method is particularly prone to error because *foF2* is taken as unknown and $\partial N/\partial h$ at one of the two measuring points is required in the extrapolation to determine it. As a general rule, *foF2* can be measured directly off the ionogram much more correctly than it can be determined by Jackson's method. A 1 per cent error in *foF2* is equivalent to over 20 per cent error in semi-thickness (Piggott, 1954) and thus the *hcqc* analysis is probably more accurate than Jackson's for the fourth case in the table.

Using the "*hcqc*" method, 80 high-quality ionograms recorded at the Argentine Islands between December 1967 and January 1969 have been reduced. Of this sample, approximately half were from summer months and the remainder were split between winter and equinox. The period covered by the sample was representative of median sunspot activity. To test for solar cycle sensitivity, a further six ionograms recorded in December 1957 (sunspot maximum) and seven ionograms from December 1963 (sunspot minimum) were included.

3. *The parameters and their measuring uncertainty*

The primary parameters measured from the ionograms are listed in Table IV. This table gives the estimated measuring uncertainties in these parameters for this analysis and also those agreed on internationally (Piggott and Rawer, 1972).

TABLE IV
MEASURING UNCERTAINTIES IN THE PRIMARY PARAMETERS

Parameter	*foF2* (MHz)	*foE* (MHz)	*MUF* (per cent)	*h'F(F2)* (km.)	*hcF2* (km.)	*qcF2* (km.)
Measuring uncertainty used	0·05	0·05	1	5	10	5
International uncertainty	0·1	0·05	*	5	†	†

* $M(3000)F2\left(=\frac{MUF}{foF2}\right)$ is quoted; the uncertainty is 0·05.
† Not quoted.

From these primary parameters, the working set was obtained from the equations given in Table V. The equations for the most probable uncertainty are also given in this table.

TABLE V
DEFINITIONS OF WORKING PARAMETERS

Parameter definition	*Uncertainty relation*
$x_E = \frac{foF2}{foE}$	$\delta x_E = \pm x_E\left\{\left(\frac{\delta foF2}{foF2}\right)^2+\left(\frac{\delta foE}{foE}\right)^2\right\}^{\frac{1}{2}}$
$M_0 = \frac{MUF}{foF2}$	$\delta M_0 = \pm M_0\left\{\left(\frac{\delta foF2}{foF2}\right)^2+\left(\frac{\delta MUF}{MUF}\right)^2\right\}^{\frac{1}{2}}$
$M_T = \frac{1490}{hcF2+176}$	$\delta M_T = \pm\frac{M_T}{hcF2+176}\delta hcF2$
$ycF2 = 2qcF2$	$\delta ycF2 = \pm 2\delta qcF2$
$hpF2 = \frac{1490}{M_0}-176$	$\delta hpF2 = \pm\frac{1490}{M_0^2}\delta M_0$
$\Delta M = M_T - M_0$	$\delta\Delta M = \pm\{(\delta M_T)^2+(\delta M_0)^2\}^{\frac{1}{2}}$
$\Delta h = hpF2 - hcF2$	$\delta\Delta h = \pm\{(\delta hpF2)^2+(\delta hcF2)^2\}^{\frac{1}{2}}$
$ho = hcF2 - ycF2$	$\delta ho = \pm\{(\delta hcF2)^2+(\delta ycF2)^2\}^{\frac{1}{2}}$
$\eta = \frac{ycF2}{ho}$	$\delta\eta = \pm\eta\left\{\left(\frac{\delta ycF2}{ycF2}\right)^2+\left(\frac{\delta ho}{ho}\right)^2\right\}^{\frac{1}{2}}$

It is unnecessary to compute the uncertainties for each parameter for every ionogram analysed. Indeed this would be a futile exercise since the uncertainties given in Table IV are only average values. An adequate appreciation of the importance of the measuring uncertainties may be obtained by looking in detail at a small sample of data. To this end, five cases have been selected, three from summer (1 to 3) and two from winter (4 and 5), representative of median sunspot activity. The primary parameters scaled in these cases are given in Table VI.

TABLE VI
PRIMARY PARAMETERS USED FOR ESTIMATION OF UNCERTAINTIES

Case	*foF2*	*foE*	*MUF*	*hcF2*	*qcF2*
1	11·25	2·75	30·0	361	60
2	7·90	3·45	20·2	363	70
3	6·00	3·70	15·1	301	50
4	4·40	1·85	14·5	252	35
5	6·85	1·70	26·0	221	20

The working parameters computed from this set are listed in Table VII. The following general conclusions may be drawn:

i. In summer the uncertainty in x_E is approximately $\pm$ 2 per cent, whereas that in ΔM is roughly independent of ΔM and is of the order $\pm$ 0·06 to $\pm$ 0·07; further, the uncertainty in Δh is independent of Δh and is approximately $\pm$ 12 km. The uncertainty in x_E is generally insignificant compared with the others.

ii. In winter, the uncertainties in x_E and ΔM are both increased because of seasonal changes in *foF2*, *foE* and *hcF2*. However, seasonal variations in *M(3000)F2* cancel in the calculation of the variability of $\delta(\Delta h)$ so that this parameter remains the same as in summer.

Overall, the uncertainties in ΔM and Δh are far more important than those in x_E and are both roughly constant.

TABLE VII

WORKING PARAMETERS COMPUTED USING THE DATA IN TABLE VI

Parameter	*Summer*			*Winter*	
	1	2	3	4	5
x_E	4·091 ± 0·077	2·290 ± 0·057	1·622 ± 0·026	2·38 ± 0·07	4·03 ± 0·12
M_0	2·667 ± 0·032	2·557 ± 0·030	2·517 ± 0·033	3·295 ± 0·050	3·796 ± 0·047
M_T	2·775 ± 0·052	2·764 ± 0·051	3·124 ± 0·065	3·481 ± 0·081	3·753 ± 0·095
ΔM	0·108 ± 0·061	0·207 ± 0·059	0·607 ± 0·073	0·186 ± 0·095	−0·04 ± 0·11
hpF2	383 ± 7	407 ± 7	416 ± 8	276 ± 7	217 ± 5
Δh	22 ±12	44 ±12	115 ±13	24 ±12	− 4 ±11
ycF2	120 ±10	140 ±10	100 ±10	70 ±10	40 ±10
ho	241 ±14	223 ±14	201 ±14	182 ±14	181 ±14
η	0·498 ± 0·051	0·628 ± 0·060	0·498 ± 0·061	0·385 ± 0·063	0·221 ± 0·058

4. *Sensitivity to changes in yp/ho*

The value of *hp* determined from *M(3000)F2* depends upon the ratio *yp/ho*. This term, approximated by the parameter η as defined in Table V, is an uncontrolled variable in the data sample. The analysis on p. 10 suggests that the effects of variations in this term should be small, but it is necessary to test whether the error introduced is significant compared with that due to measuring inaccuracies. It is also important to assess to what extent systematic inconsistencies are introduced between blocks of data due to seasonal variations in *yp/ho*.

Although it is necessary to use Shimazaki's equation for evaluating *hp* and ΔM, it is not desirable to use his theory for the required tests. The approximate approach adopted by Shimazaki does not reveal the dependence on *yp* and *ho* in its simplest form but introduces these parameters separately in a cumbersome fashion. A third parameter, ζ, is also introduced (p. 14) whose seasonal and diurnal variations would produce changes of the same order as the expected effects due to *yp/ho*. It has already been demonstrated that the main effect of Shimazaki's approximations is to make the apparent *yp/ho* smaller when compared with Appleton–Beynon theory. Otherwise, the variation of *hp* with *M(3000)F2* is very similar in the two cases. Thus, the Appleton–Beynon theory can be used to give a reasonable indication of the likely effects of variability in *yp/ho*.

Referring to Equation (22), "Appleton–Beynon" analysis gives

$$hpF2 = a'\left[\frac{1}{M_0{}^2-1}\right]^{\frac{1}{2}} - b',$$

where a' and b' are functions of *yp/ho*. If ΔM is the required correction for underlying ionization and $M_T = M_0 + \Delta M$, it follows

$$hcF2 = a'\left(\frac{1}{M_T{}^2-1}\right)^{\frac{1}{2}} - b', \qquad (47)$$

which may be inverted to give

$$M_T = \left[\left(\frac{a'}{hc+b'}\right)^2+1\right]^{\frac{1}{2}},$$

from which it follows

$$\Delta M = \left[\left(\frac{a'}{hc+b'}\right)^2+1\right]^{\frac{1}{2}}-M_0. \tag{48}$$

Consider the general case where the true ΔM is ΔM_1, for a particular x_E, when $M_0 = M_1$, $hc = h_1$ and η ($= yc/ho$) is η_1. In this case let the coefficients be a'_1 and b'_1. For the corresponding case, when $\eta = \eta_2$ but x_E remains the same, let the variables be suffixed by 2. Then the difference between the two computed ΔM's (a measure of the induced error) is given by

$$\Delta M_1-\Delta M_2 = (M_2-M_1)+\left[\left(\frac{a'_1}{h_1+b'_1}\right)^2+1\right]^{\frac{1}{2}}-\left[\left(\frac{a'_2}{h_2+b'_2}\right)^2+1\right]^{\frac{1}{2}}. \tag{49}$$

Consider the case of the summer block of data; the median value of $\eta = 0{\cdot}56$ (48 observations) with upper quartile $0{\cdot}64$ and lower quartile $0{\cdot}50$. To assess the noise inherent in this sample, it is reasonable to suppose that $M_1 = M_2$, $h_1 = h_2$ and then evaluate Equation (49) for the two quartile values of η for chosen heights.

By interpolation from Table I, the required values of the coefficients are

$$\eta = 0{\cdot}50,\ a'_1 = 1164, \quad \eta = 0{\cdot}64,\ a'_2 = 1151,$$
$$b'_1 = 105; \qquad b'_2 = 101.$$

Then, for the typical summer values of *hcF2* listed below, Equation (49) gives

$$hcF2 = 300 \text{ km.} \quad \Delta M_1-\Delta M_2 = 0{\cdot}004$$
$$hcF2 = 350 \text{ km.} \quad \Delta M_1-\Delta M_2 = 0{\cdot}006$$
$$hcF2 = 400 \text{ km.} \quad \Delta M_1-\Delta M_2 = 0{\cdot}007.$$

Clearly, from these figures, the effect of *yp/ho* variability in the block is insignificant when compared with the noise due to errors in measurement (which is of the order of $\pm\ 0{\cdot}06$ to $\pm\ 0{\cdot}07$).

To make a valid test between blocks of winter and summer data, it is necessary to use values of M_0 and *hc* typical of the two seasons in Equation (49). Suitable values of M_0 can be chosen and, by selecting a particular value of ΔM ($0{\cdot}3$ say), the *hc*'s are found from Equation (47) using the combined summer and winter median value of η to give the coefficients.

From the data the combined median $\eta = 0{\cdot}53$, giving $a' = 1159$, $b' = 104$. Let M_0 be $2{\cdot}50$ in summer and $3{\cdot}50$ in winter, giving the corresponding values of M_T as $2{\cdot}80$ and $3{\cdot}80$. It follows that *hcF2* is 339 and 212 km., respectively. The median value of η for the winter block of data is $0{\cdot}38$. Using this with the median value for the summer data, the corresponding values of the coefficients are

$$\eta_1 = 0{\cdot}38,\ a'_1 = 1184, \quad \eta_2 = 0{\cdot}56\ a'_2 = 1157,$$
$$b'_1 = 110; \qquad b'_2 = 103.$$

Substituting these values in Equation (49) gives $\Delta M_1-\Delta M_2 = 0{\cdot}008$. This value is also small compared with the noise level and it can therefore be concluded that any effects due to changes in *yp/ho* will be masked by inaccuracies in the measurement of the primary parameters.

5. *Choice of correction parameter*

It has been pointed out that two possible methods of correcting for underlying ionization exist; the "Δh" method, in which the correction does not vary with *hmF2*; and the "ΔM" method, where the height correction increases with *hmF2*. It is suggested here that the latter approach will fit the experimental facts more precisely. To test this suggestion, some relations must first be established.

a. *ΔM invariant.* Suppose that for a particular x_E, ΔM is constant for all *hmF2*, then the expression

$$M_T = M_0+\Delta M \tag{50}$$

gives a straight line of slope unity and intercept ΔM. Equation (50) can be re-arranged to give

$$M_0 = M_T\left[1-\frac{\Delta M}{M_T}\right]$$

or

$$\frac{1}{M_0} = \frac{1}{M_T}\left[1-\frac{\Delta M}{M_T}\right]^{-1}.$$

Expressing M_T and M_0 in terms of *hcF2* and *hpF2* via Shimazaki's equation

$$hp+176 = (hc+176)\left[1-\frac{\Delta M(hc+176)}{1490}\right]^{-1},$$

therefore

$$hp = (hc+176)\left[1-\frac{\Delta M(hc+176)}{1490}\right]^{-1}-176. \tag{51}$$

Thus when ΔM is invariant, the variation of *hp* as a function of *hc* cannot be a straight line of slope unity.

b. *Δh invariant.* If Δh is constant for all *hmF2*, the equation

$$hp = hc+\Delta h \tag{52}$$

gives a straight line of unity slope and intercept Δh. The corresponding non-linear variation of M_T with M_0 is given by

$$M_T = M_0\left[1-\frac{\Delta h M_0}{1490}\right]^{-1}. \tag{53}$$

To test whether condition (a) or condition (b) pertains, two groups have been sorted from the data; the first contains all data for which $1\cdot72 \leqslant x_E \leqslant 2\cdot00$ and the second all data for which $2\cdot30 \leqslant x_E \leqslant 2\cdot70$. The mean values of Δh and ΔM for the two groups have been calculated and used in Equations (50) to (53) to give the predicted variations of *hp* versus *hc* and M_T versus M_0. These predictions have then been compared with the observed variations (see Fig. 13a–d) and the best straight-line fits to the data points have also been determined. Notice how closely the predicted variations of *hp* with *hc* (ΔM invariant) agree with the best-fit lines. For completeness the results of the regression analysis are given:

$$\begin{aligned}
1\cdot72 \leqslant x_E \leqslant 2\cdot00 \quad M_T &= (1\cdot03\pm0\cdot11)M_0 + (\ 0\cdot33\pm\ 0\cdot30)\\
hp &= (1\cdot32\pm0\cdot13)hc\ -(23\cdot7\pm40\cdot4)\\
2\cdot30 \leqslant x_E \leqslant 2\cdot70 \quad M_T &= (0\cdot99\pm0\cdot02)M_0 + (\ 0\cdot23\pm\ 0\cdot06)\\
hp &= (1\cdot15\pm0\cdot03)hc\ -(11\cdot0\pm11\cdot0),
\end{aligned}$$

which should be compared with those expected with:

a. ΔM invariant

$$\begin{aligned}
1\cdot72 \leqslant x_E \leqslant 2\cdot00 \quad M_T &= M_0+0\cdot41\\
2\cdot30 \leqslant x_E \leqslant 2\cdot70 \quad M_T &= M_0+0\cdot20.
\end{aligned}$$

b. Δh invariant

$$\begin{aligned}
1\cdot72 \leqslant x_E \leqslant 2\cdot00 \quad hp &= hc\ +73\\
2\cdot30 \leqslant x_E \leqslant 2\cdot70 \quad hp &= hc\ +41.
\end{aligned}$$

It is clear from this analysis that the "ΔM" method is superior to the "Δh" method.

6. *ΔM as a function of x_E*

The values of ΔM as a function of x_E, determined from 80 ionograms representative of median sunspot activity are shown graphically in Fig. 14. The data are divided into three groups by season. Almost all the summer ionograms showed well-defined *F1*-layer characteristics but these were entirely absent in the other two seasonal groups. The following points are evident from the figure:

i. A smooth variation of ΔM with x_E can be established empirically from low to high values of x_E.
ii. There are no systematic discrepancies between the summer and equinox data, indicating that the influence of the presence or absence of an *F1*-cusp is negligible.
iii. In summer a number of cases occur for which x_E is less than the Bradley and Dudeney limit of 1·7.
iv. The scatter of the summer and equinox data seems consistent with the value expected from measuring inaccuracies alone.

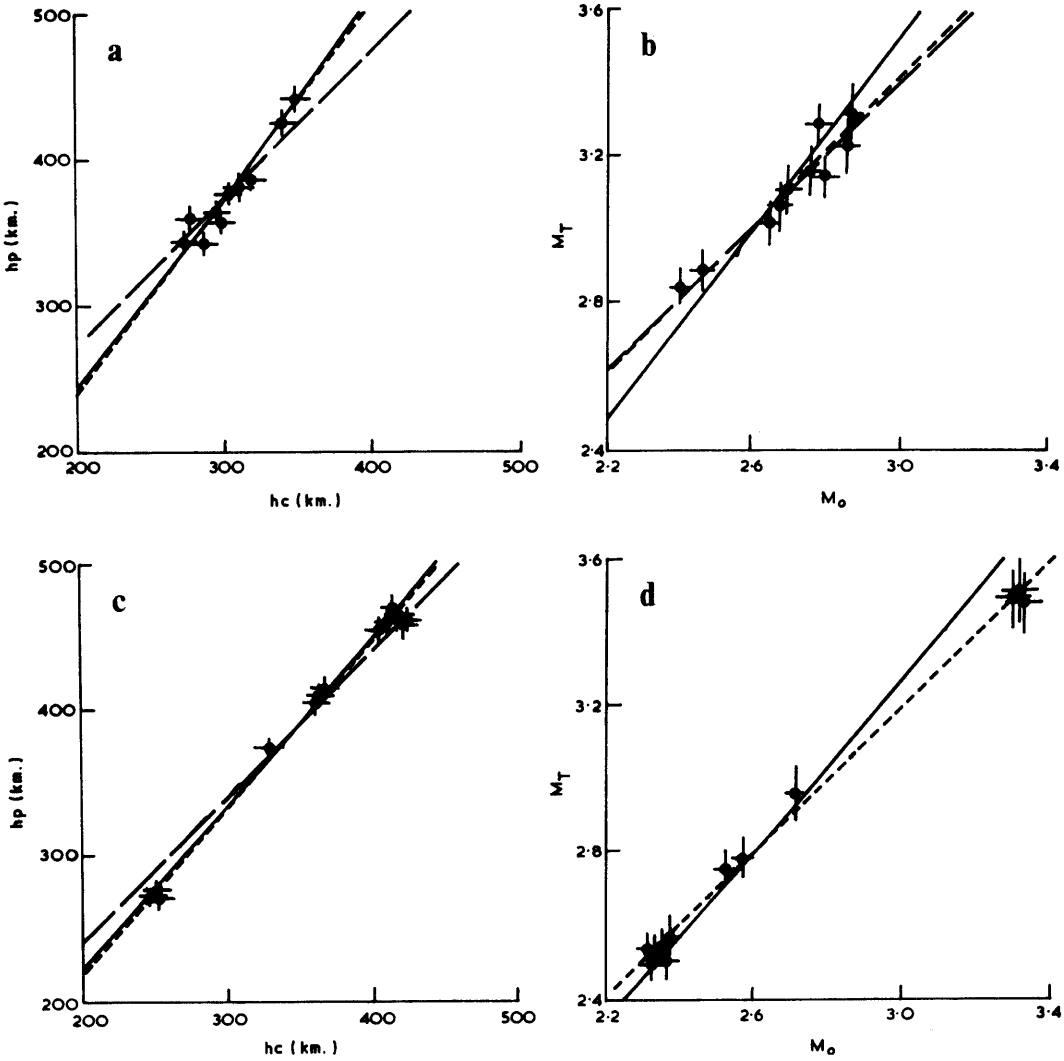

FIGURE 13

Comparison of the "Δh" and "ΔM" correction methods.

a and b. $1{\cdot}72 \leqslant x_E \leqslant 2{\cdot}00$.

a. Long-dashed line, Equation (52) with $\Delta h = 73$ km. Solid line, Equation (51) with $\Delta M = 0{\cdot}41$. Short-dashed line, best fit to data points.

b. Long-dashed line, Equation (50) with $\Delta M = 0{\cdot}41$. Solid line, Equation (53) with $\Delta h = 73$ km. Short-dashed line, best fit.

c and d. $2{\cdot}30 \leqslant x_E \leqslant 2{\cdot}70$.

c. As for (a) but with $\Delta h = 41$ km. and $\Delta M = 0{\cdot}20$.

d. As for (b) but with $\Delta M = 0{\cdot}20$ and $\Delta h = 41$ km.

For case (d), the best fit and the ΔM invariant line coincide, so only the former is shown.

v. The winter data form a separate family whose values are depressed, compared with the summer and equinox ones. Note that the magnitude of this depression is considerably larger than can be accounted for by seasonal changes in yp/ho.

A suitable equation of best fit to the data would be that of a rectangular hyperbola of the form

$$\Delta M = \frac{A}{x_E - B} + C, \tag{54}$$

which is asymptotic to $x_E = B$ at $\Delta M = \infty$, and asymptotic to $\Delta M = C$ at $x_E = \infty$. If the true height of the layer had been exactly determined and all factors influencing the path of the ray to its

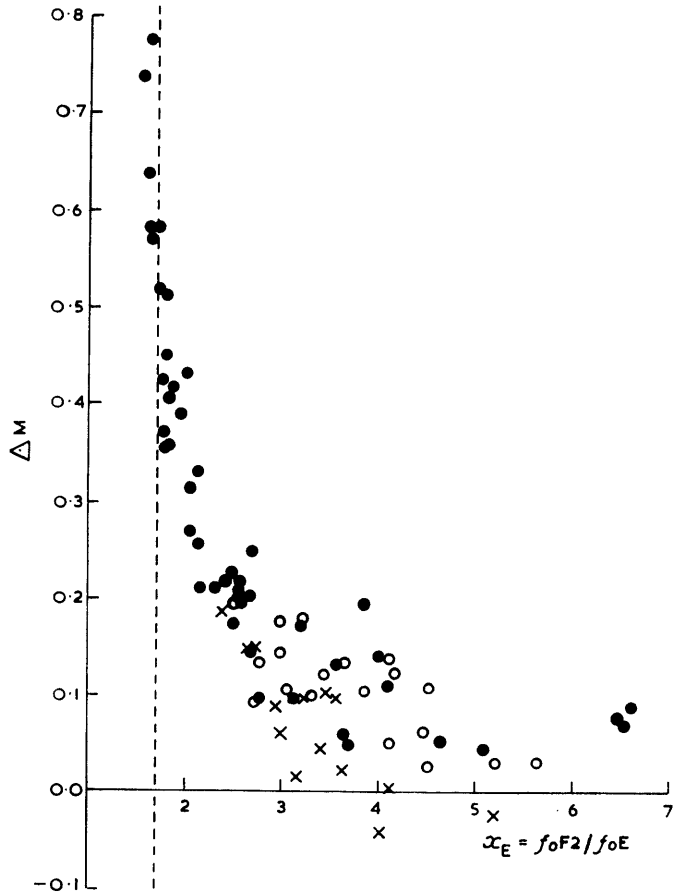

FIGURE 14

The variation of ΔM as a function of x_E, determined from 80 ionograms recorded at the Argentine Islands in the period 1967–69. Solid circles: summer; open circles: equinox; crosses: winter. The vertical dashed line marks $x_E = 1{\cdot}7$.

reflection point were included, we would expect $C = 0$ from the analysis. Physically, ΔM does not approach infinity as x_E becomes small but becomes indeterminant when M_0 becomes unmeasurable. It is probable that ΔM approaches some finite limit of the order of M_T, but the error introduced by assuming the infinite limit is small.

These points are now investigated quantitatively by performing the best-fit analysis suggested above. Because Equation (54) involves three unknowns, the following procedure is adopted:

i. Choose a value for B.
ii. Find the coefficients of the line of best fit, and correlation coefficient, R, for ΔM as a function of X, where X is given by $(x_E - B)^{-1}$.
iii. Repeat step (ii) with a new value of B until the maximum value of the correlation coefficient is obtained. Use the coefficients applicable to this value.

The sensitivity of R to changes in B will be an inverse function of the noise within the data. In the present case R changed relatively slowly with B, a variation of $\pm 0{\cdot}005$ in the latter about the best values only altered R by $\pm 0{\cdot}0001$. However, this range of uncertainty in B is not of any importance since, whilst a slight change of B alters A and C, it does so in such a way that the predicted values of ΔM remain essentially unchanged.

Table VIII gives the results of this procedure applied to the data in Fig. 14. In this table, R is the maximum value of the correlation coefficient and S is the standard deviation of the points about the best line.

Notice, from the table, that for summer and equinox C is very close to zero as expected. Also, S is of the same order as the estimated uncertainties in the individual data points. This suggests that the noise in the

TABLE VIII
RESULTS OBTAINED BY BEST FITTING EQUATION (54) TO THE DATA IN FIG. 14

Data sample	*A*	*B*	*C*	*R*	*S*
Summer only	0·247±0·010	1·225	0·005±0·010	0·962	0·053
Summer and equinox	0·250±0·008	1·225	0·000±0·010	0·964	0·048
Summer, equinox and winter	0·280±0·009	1·200	−0·028±0·010	0·957	0·052

data is mainly due to measuring inaccuracies and that there are no significant systematic effects (apart from the winter disagreement) which have not been accounted for.

The summer, and the summer plus equinox data are described by essentially the same set of coefficients, in agreement with the qualitative conclusion reached above. Also the addition of the winter data alters the values significantly. Although the equation obtained from all the data combined is probably adequate for the present purpose, it is informative to investigate the causes of the winter disagreement, which is discussed below.

7. *The winter disagreement*

It has already been noted that systematic seasonal changes in η cannot account for the anomaly because the modifications thereby introduced are too small. A more likely cause is inadequacy of the $1/M$ approximation used by Shimazaki to simplify his equation. For winter, the median value of M is 3·4, whilst for summer it is 2·6. Fig. 9 indicates that use of the approximation introduces discrepancies of −4 and +4 km. for these values of M. These are in the correct sense to account for the anomaly.

To show that this explanation provides the answer, the values of ΔM have been recalculated using the Shimazaki expression in its complete form

$$hpF2 = \frac{1490\ (M_0F)}{M_0} - 176,$$

from which it follows

$$hcF2 = \frac{1490\ (M_0F)}{M_T} - 176,$$

therefore

$$M_T = \frac{1490\ (M_0F)}{hc+176},$$

and finally

$$\Delta M = \frac{1490\ (M_0F)}{hc+176} - M_0.$$

Fig. 15a gives the original values of ΔM for $x_E > 2$, whilst in Fig. 15b the results of this re-analysis are presented. The best-fit curves are also given: on re-analysis the coefficients become $A = 0{\cdot}253 \pm 0{\cdot}008$, $B = 1{\cdot}215$ and $C = -0{\cdot}012 \pm 0{\cdot}009$. The standard deviation, σ_m, defined as

$$\sigma_m = \left[\sum_{i=1}^{n} \frac{(\Delta M_i - ((A/x_E - B) + C))^2}{n-1}\right]^{\frac{1}{2}}$$

has been calculated, for the range $2{\cdot}30 \leqslant x_E \leqslant 6{\cdot}00$, for the cases given in Table IX. The range in x_E was

TABLE IX
RE-ANALYSIS USING THE COMPLETE FORM OF SHIMAZAKI'S EQUATION

	All data	*Summer*	*Equinox*	*Winter*
Full analysis	0·039	0·040	0·037	0·043
Approximate analysis	0·047	0·047	0·038	0·059

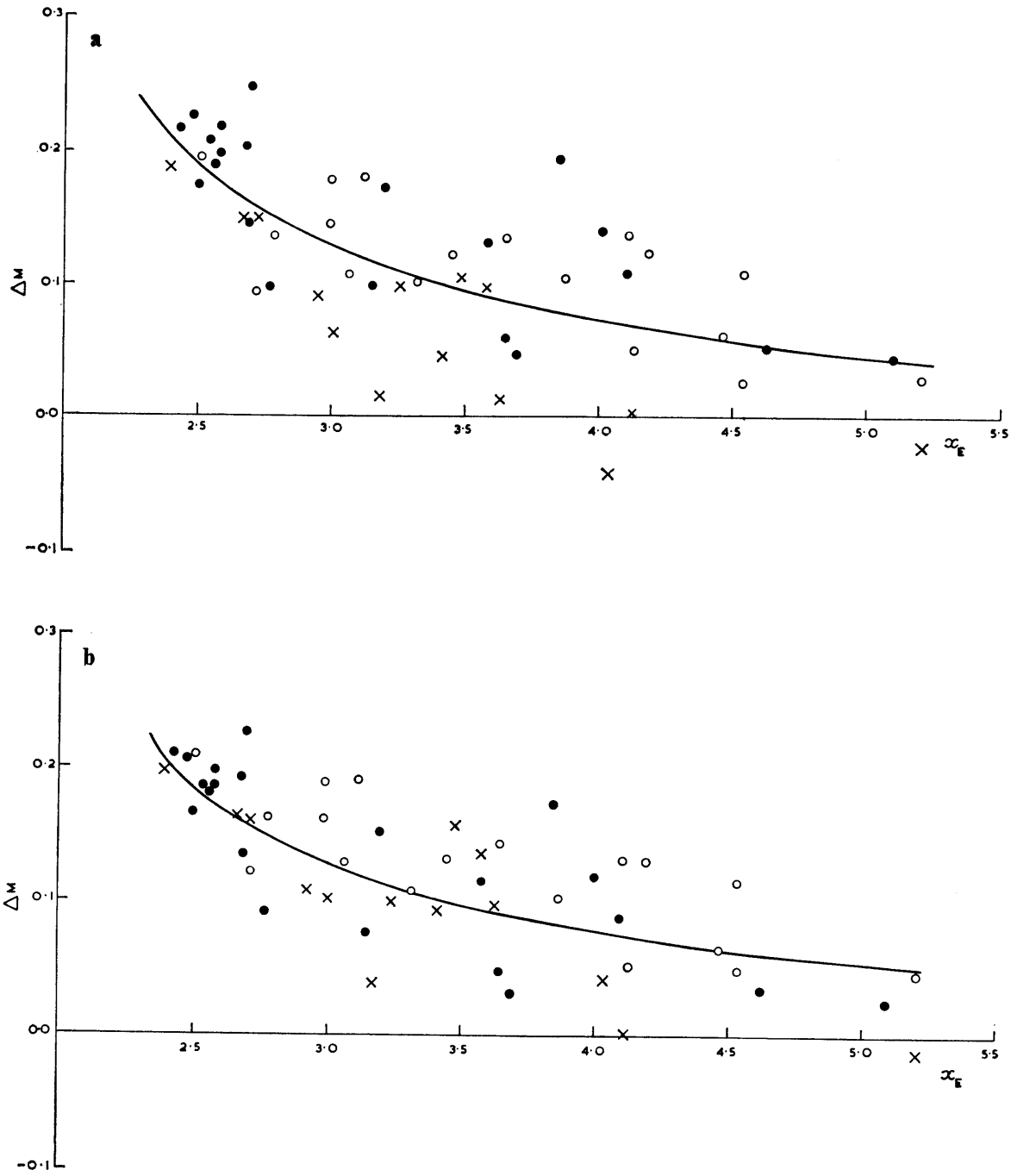

FIGURE 15

The anomalous behaviour of winter data.

a. The original data showing anomaly.
b. The same data after the distortion due to the $1/M$ approximation has been removed.
Solid circles: summer; open circles: equinox; crosses: winter; curves: best fit to Equation (54) for each sample but over the whole range of x_E.

chosen to just include all the winter and equinox data without including extraneous summer data well away from the winter–equinox data block.

Notice that σ_m for equinox remains essentially unchanged, whereas it is substantially reduced for the other two seasons by re-analysis. The equinox result is perfectly understandable because the median value of M_0 for this season is such that the error is zero.

8. *The equations for $\dot{h}mF2$*

The question arises as to whether the inclusion of the more complete equation for *hpF2* produces differences in the calculated values of $\dot{h}mF2$ sufficient to warrant the added complexity. The coefficients given in Table VIII and those calculated in the previous sub-section give two sets of equations for $\dot{h}mF2$:

$$\left.\begin{aligned} \dot{h}mF2 &= \frac{1490}{M(3000)F2+\Delta M}-176 \\ \Delta M &= \frac{0{\cdot}280\pm0{\cdot}009}{x_E-1{\cdot}200}-(0{\cdot}028\pm0{\cdot}010) \\ x_E &= \frac{foF2}{foE}, \end{aligned}\right\} \tag{55}$$

or

$$\left.\begin{aligned} \dot{h}mF2 &= \frac{1490\ (M.F)}{M(3000)F2+\Delta M}-176 \\ (M.F) &= M(3000)F2\left(\frac{0{\cdot}0196\ M(3000)F2^2+1}{1{\cdot}2967\ M(3000)F2^2-1}\right)^{\frac{1}{2}} \\ \Delta M &= \frac{0{\cdot}253\pm0{\cdot}008}{x_E-1{\cdot}215}-(0{\cdot}012\pm0{\cdot}009) \\ x_E &= \frac{foF2}{foE}. \end{aligned}\right\} \tag{56}$$

The values of $\dot{h}mF2$ predicted by these two sets are compared (Fig. 16) by plotting the difference: $\dot{h}m$ (Equation (55))$-\dot{h}m$ (Equation (56)) as a function of x_E parametric in $M(3000)F2$. The figure indicates

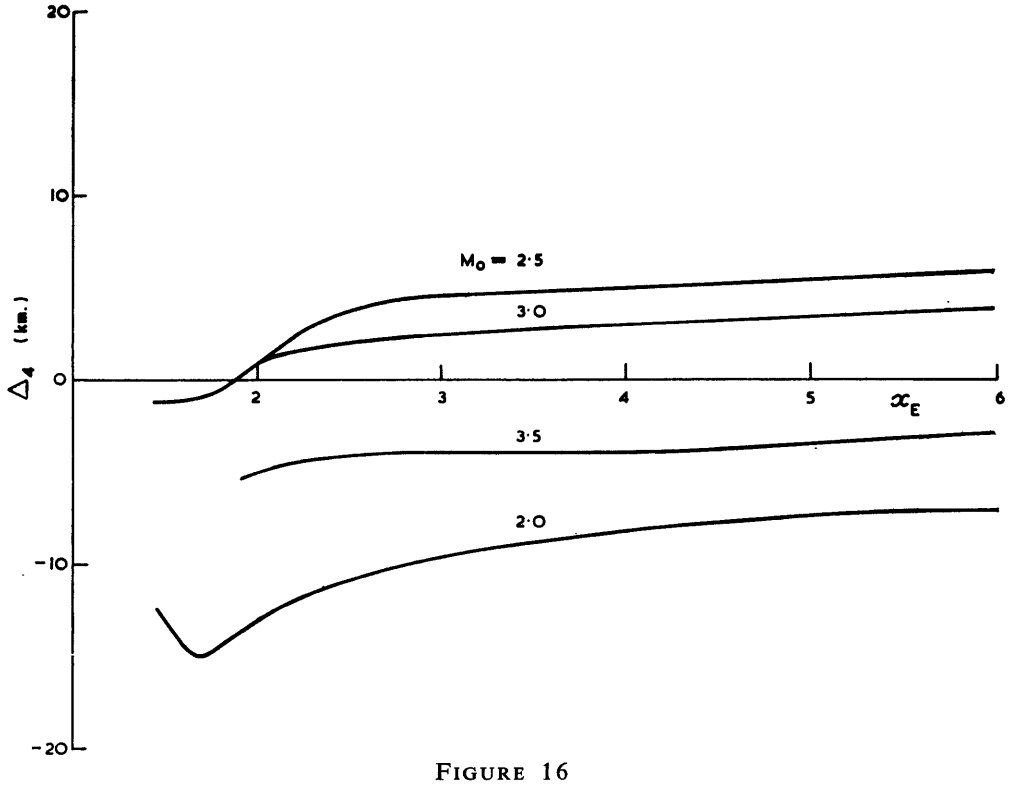

FIGURE 16

Comparison of the complete and simplified $(1/M)$ formulations for $\dot{h}mF2$. The figure gives the difference $\Delta_4 = \dot{h}m$ (Equation 55)$-\dot{h}m$ (Equation 56) as a function of x_E and parametric in M_0.

that the differences between the two sets of equations are barely significant for most values of *M(3000)F2* but become more important when *M(3000)F2* becomes small. Thus for some applications the simple formulation (Equation (55)) may be adequate, but for studies such as the solar-cycle variations in $h\dot{m}F2$, where extreme values of *M(3000)F2* can be expected, the more complex relationships (Equations (56)) must be used. Where a computer can be employed, the added complexity is not significant; for manual analysis, on the other hand, the relationships are rather cumbersome. For this reason a chart (Fig. 17) has been constructed from Equation (56) giving $h\dot{m}F2$ as a function of x_E parametric in *M(3000)F2*. From this chart $h\dot{m}F2$ may be determined with adequate accuracy for a wide range of practical cases.

9. *Uncertainty in the predicted value of* $h\dot{m}F2$

A full treatment of the uncertainties in $h\dot{m}F2$ derived from Equation (56) would be cumbersome and would not produce results significantly at variance with those obtainable more easily from Equation (55). The latter equation will be used in the following analysis, but the results should apply equally to the former. Thus

$$h\dot{m}F2 = \frac{1490}{M_T} - 176, \tag{57}$$

where

$$M_T = M_0 + \frac{A}{x_E - B} + C. \tag{58}$$

Differentiating Equation (57)

$$\frac{\mathrm{d}h\dot{m}}{\mathrm{d}M_T} = -\frac{1490}{M_T{}^2},$$

Therefore

$$\delta h\dot{m}F2 \simeq \pm\frac{1490}{M_T{}^2}\delta M_T. \tag{59}$$

Now $M_T = f(M_0, x_E, A, C)$ with B assumed fixed,

so that

$$\delta M_T = \frac{\partial M_T}{\partial M_0}\delta M_0 + \frac{\partial M_T}{\partial x_E}\delta x_E + \frac{\partial M_T}{\partial A}\delta A + \frac{\partial M_T}{\partial C}\delta C.$$

It follows by differentiating Equation (58) by parts

$$\delta M_T = \delta M_0 - \frac{A\delta x_E}{(x_E - B)^2} + \frac{\delta A}{x_E - B} + \delta C.$$

Substituting in Equation (59)

$$\delta h\dot{m}F2 = \pm\frac{1490}{M_T{}^2}\left[\delta M_0 + \delta C + \frac{\delta A}{x_E - B} - \frac{A\delta x_E}{(x_E - B)^2}\right].$$

The most probable error is given by

$$\overline{\delta h\dot{m}F2} = \pm\frac{1490}{M_T{}^2}\left[\left\{\delta M_0 + \delta C + \frac{\delta A}{x_E - B}\right\}^2 + \left\{\frac{A\delta x_E}{(x_E - B)^2}\right\}^2\right]^{\frac{1}{2}}. \tag{60}$$

Substitution of the values of the coefficients from Table VIII gives

$$\overline{\delta h\dot{m}F2} = \pm\frac{1490}{(M_0 + \Delta M)^2}\left[\left\{\delta M_0 + 0{\cdot}01 + \frac{0{\cdot}009}{x_E - 1{\cdot}2}\right\}^2 + \left\{\frac{0{\cdot}28\delta x_E}{(x_E - 1{\cdot}2)^2}\right\}^2\right]^{\frac{1}{2}}. \tag{61}$$

The equation for δx_E is given in Table V.

Since the purpose of the analysis is to determine *hmF2* from standard parameters, it is clearly worthwhile to incorporate the internationally recognized uncertainty limits (Table IV) into Equation (61), which then becomes

$$\overline{\delta h\dot{m}F2} = \frac{1490}{(M_0 + \Delta M)^2}\left[\left\{0{\cdot}06 + \frac{0{\cdot}009}{(x_E - 1{\cdot}2)}\right\}^2 + \left\{\frac{0{\cdot}28\,\delta x_E}{(x_E - 1{\cdot}2)^2}\right\}^2\right]^{\frac{1}{2}}. \tag{62}$$

Thus the height error is a function of M_0, x_E, *foF2* and *foE* (the latter two parameters control δx_E at constant x_E). However, it is clear, for all practical values of x_E and δx_E, that

$$0{\cdot}06 \gg \frac{0{\cdot}009}{x_E - 1{\cdot}2}$$

and

$$0{\cdot}06 \gg \frac{0{\cdot}28\,\delta x_E}{(x_E - 1{\cdot}2)^2} \text{ except when } x_E \text{ is small.}$$

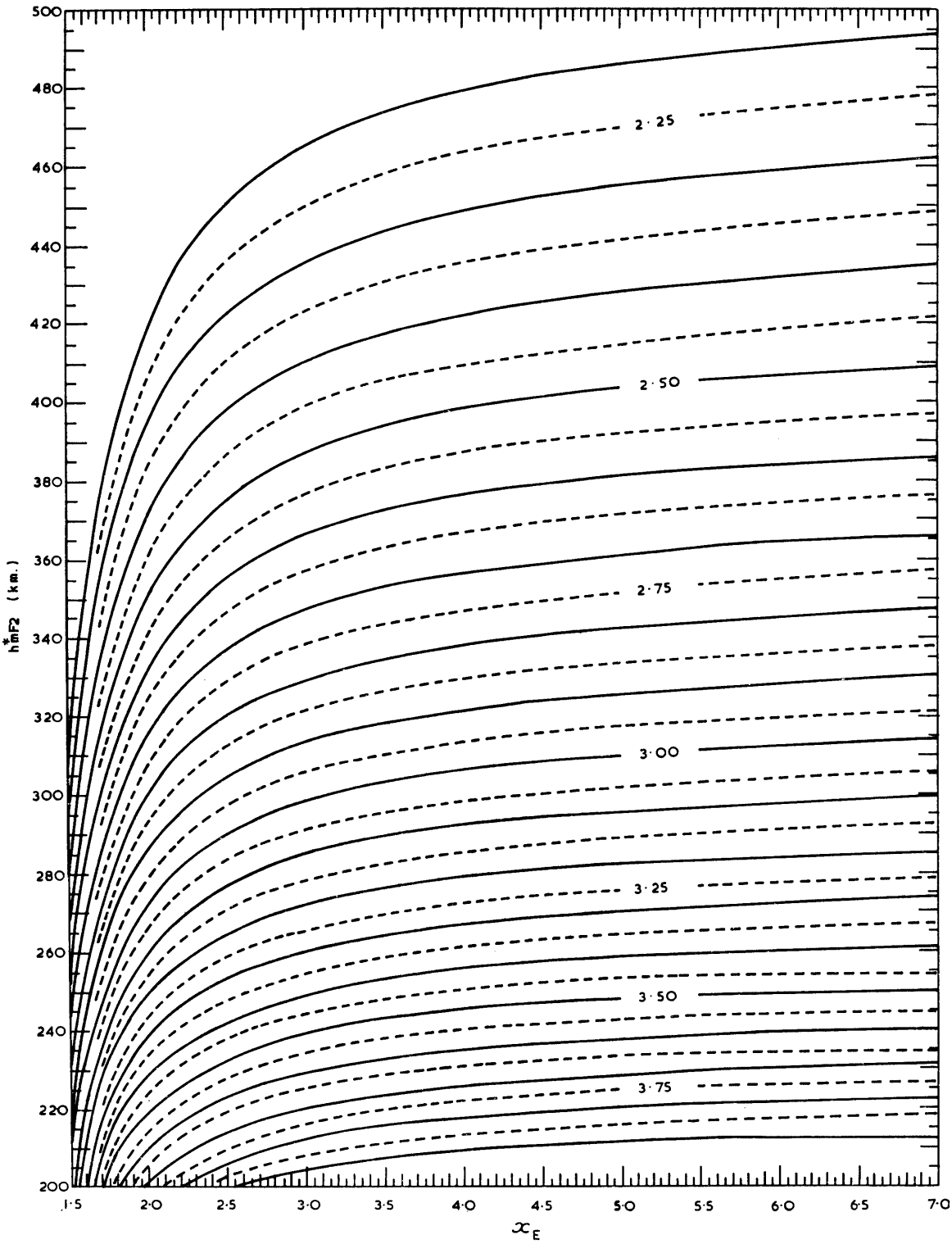

FIGURE 17

A useful graphical solution of Equation (56) which allows estimation of $h\dot{m}F2$, without computation, to better than $\pm 2{\cdot}5$ km.

When x_E is small, the latter term in x_E will be compensated by the ΔM term which becomes larger, so that $\overline{\delta h\dot{m}F2}$ should vary approximately as a function of M_0 alone. Sample calculations (Table X) show that this

TABLE X
ESTIMATION OF UNCERTAINTY IN $h\dot{m}F2$ ASSUMING STANDARD ACCURACY RULES

M	x_E	$foF2$	foE	$\overline{\delta h\dot{m}F2}$
2·0	2	6·0	3·0	20·5
	2	12·0	6·0	19·9
	5	5·0	1·0	22·2
	5	10·0	2·0	22·2
4·0	2	6·0	3·0	5·9
	2	12·0	6·0	5·7
	5	5·0	1·0	5·7
	5	10·0	2·0	5·7

is indeed the case. It is thus possible to give the sample representation for $\overline{\delta h\dot{m}F2}$ shown in Fig. 18, from which the height uncertainty can be estimated with reasonable assurance.
Alternatively, Equation (62) reduces to the simple form

$$\overline{\delta h\dot{m}F2} \simeq \pm\frac{89}{M_0^2}\text{ km.} \tag{63}$$

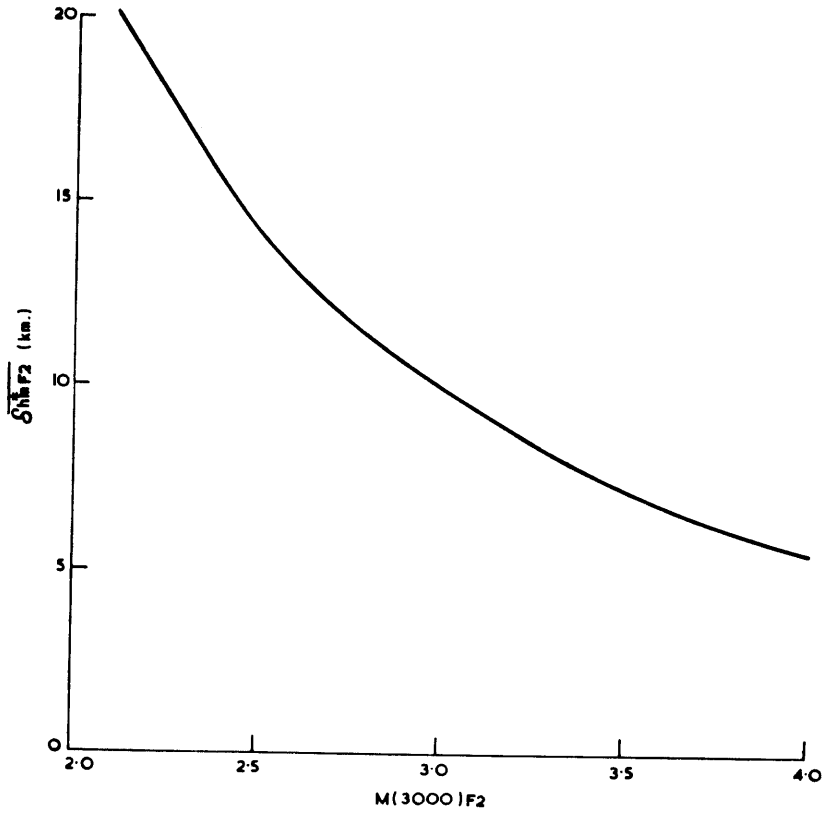

FIGURE 18
Curve giving average uncertainty in $h\dot{m}F2$ as a function of $M(3000)F2$, assuming the international accuracy rules apply.

10. *Comparisons at other epochs of the solar cycle*

The equations given above for $h\dot{m}F2$ strictly apply for median sunspot activity (10·7 cm. solar flux; $120\text{–}170\times10^{-22}$ W m.$^{-2}$ Hz^{-1}), since the data were obtained during this epoch. To test whether the same equations are applicable at other epochs of the solar cycle, sample data have been obtained from the same location for the months of December 1957 (mean 10·7 cm. solar flux = 282) and December 1963 (mean flux = 74). Great care was taken in the analysis of the sample ionograms to ensure maximum accuracy.

TABLE XI
PRIMARY PARAMETERS FOR SOLAR CYCLE COMPARISON

Date	*L.T.*	*foF2*	*foE*	*MUF*	*hcF2*
17.xii.57	07·00	8·65±0·050	3·50±0·025	19·0±0·10	445±10
17.xii.57	08·00	7·75±0·050	3·75±0·025	17·3±0·10	406±10
17.xii.57	11·00	6·40±0·025	4·10±0·075	14·0±0·10	316±10
17.xii.57	06·00	8·85±0·050	3·30±0·050	19·1±0·15	460±10
17.xii.57	19·00	6·65±0·050	3·00±0·025	15·5±0·10	392±10
28.xii.57	04·30	11·20±0·050	2·85±0·050	24·0±0·20	498±10
5.xii.63	06·00	6·45±0·025	2·50±0·050	18·6±0·10	306±10
5.xii.63	07·00	5·60±0·050	2·60±0·050	16·0±0·20	311±15
5.xii.63	08·00	5·70±0·025	2·80±0·075	17·2±0·10	281±10
5.xii.63	12·00	5·10±0·025	3·05±0·050	14·5±0·25	262±10
5.xii.63	16·00	5·20±0·025	2·80±0·025	14·0±0·20	296±10
6.xii.63	19·00	6·30±0·025	2·20±0·025	19·5±0·15	289±10
7.xii.63	08·00	5·75±0·025	2·80±0·075	17·6±0·20	272±10

Table XI lists the primary parameters so derived with estimates of measuring uncertainty. Values of $h\dot{m}F2$ determined from these parameters using Equations (56) and (61) are compared with the corresponding values of *hcF2* in Fig. 19. The agreement between the two is remarkably good, providing very convincing evidence of the superiority of the "ΔM" method over the "Δh" method. It should be recalled here that Vickers' empirical analysis using Δh required very different empirical coefficients at different epochs of the solar cycle. It is of note (see Fig. 20) that the Δh correction terms (defined by Equation (42)) approximately double in value between solar minimum and solar maximum for constant x_E.

11. *An empirical equation for* $y\dot{m}F2$

The lowest virtual height recorded from a simple parabolic layer is approximately equal to the lowest real height (*ho*). The difference between this virtual height and *hp* is thus approximately equal to *yp*. In the real ionosphere it is possible to use the lowest recorded virtual height from the *F2*-layer to estimate the semi-thickness of the equivalent parabolic *F2*-layer. In general, because of the influence of underlying layers, $h'F(F2)$ will give an overestimate of *ho*, so that

$$y\dot{m}F2 = h\dot{m}F2 - h'F(F2) + \Delta h', \tag{64}$$

where $\Delta h'$ is a height-correction term depending on the underlying ionization.

It is possible to determine the form of $\Delta h'$ experimentally by using suitable sample values of *hcF2*, *ycF2* and $h'F(F2)$ in Equation (64). In Fig. 21 $\Delta h'$, calculated in this way, is plotted as a function of x_E using the summer, winter and equinox data for 1967–69. It is clear from this figure that, whilst $\Delta h'$ must be a strong function of x_E (of the type already discussed), it cannot depend on this parameter alone since the winter–equinox data form a separate family from the summer data. Close inspection of the data reveals two differences between the seasonal groups:

i. *hcF2* is on average 100 km. higher for the summer data than for the other group.
ii. In the summer data the *F1*-ledge is always present but in equinox and winter always absent.

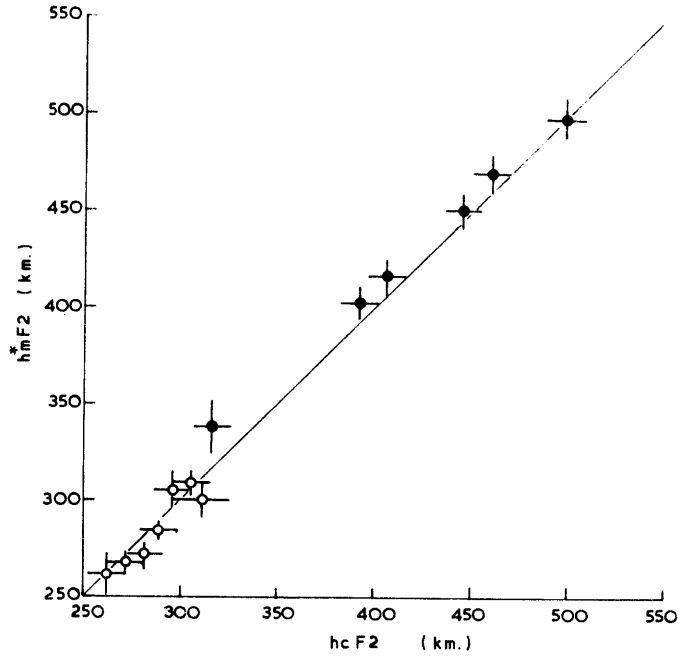

FIGURE 19

Test of Equation (56) at other epochs of the solar cycle. Open circles: sunspot minimum summer data; solid circles: sunspot maximum summer data.

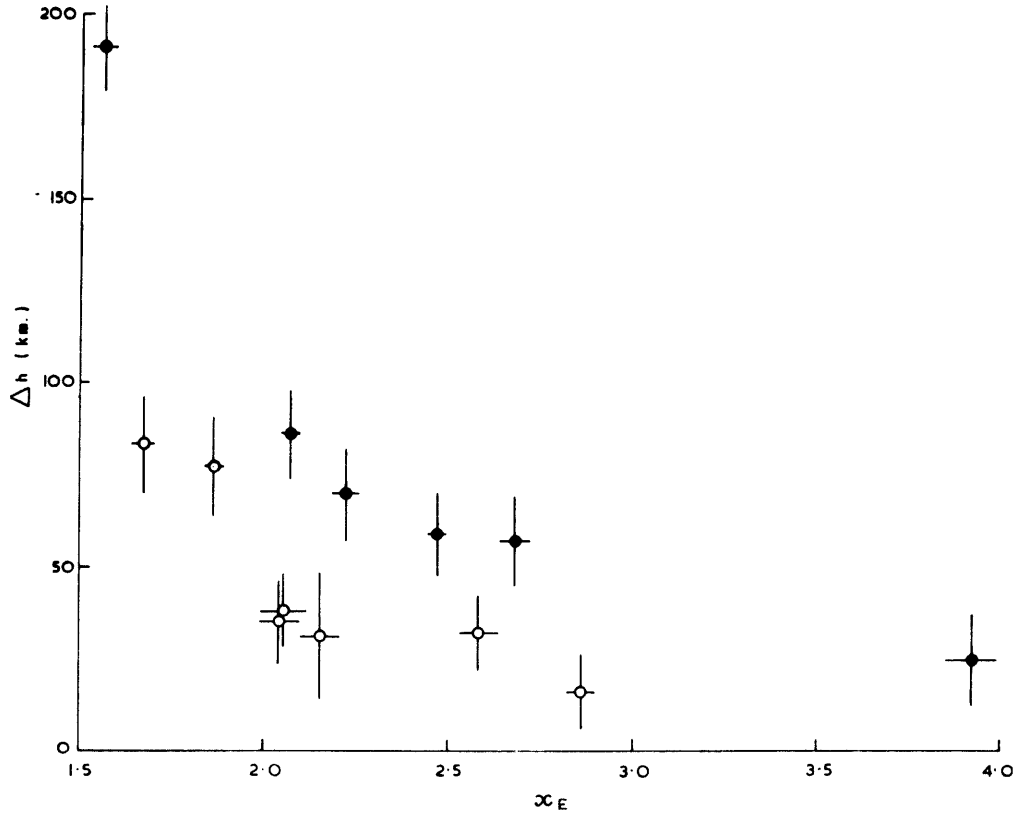

FIGURE 20

The change in magnitude of Δh at constant x_E, as a result of changes in solar activity. This figure demonstrates the difficulty of using the "Δh" correction method at different epochs of the solar cycle. Open circles: sunspot minimum summer data; solid circles: sunspot maximum summer data.

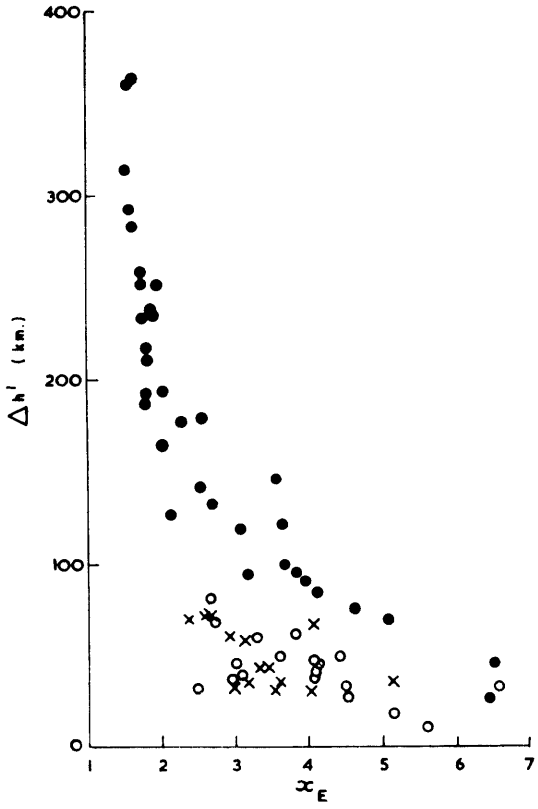

FIGURE 21

The height correction, $\Delta h'$, required to make $h'F(F2)$ a good estimate of $hoF2$, plotted as a function of x_E. Solid circles: summer data; open circles: equinox data; crosses: winter data.

From the analysis for $h\dot{m}F2$ we do not expect the latter point to be important for $h\dot{m}F2$, though it may affect $h'F2$. Bradley and Dudeney expressed $\Delta h'$ in the form

$$\Delta h' = (h\dot{m}F2 - \Lambda)\, f(x_E), \tag{65}$$

where Λ is some arbitrary constant (equal to 104 km. in the Bradley and Dudeney case). The data in Fig. 21 strongly suggest that this type of formulation is physically correct, i.e. that $\Delta h'$ is a function of the thickness of the underlying slab of ionization. The factor $h\dot{m}F2 - \Lambda$ is an indirect measure of the effective thickness of the underlying ionization profile.

An estimate of Λ for the data sample may be obtained by selecting pairs of points, one from each family, for which x_E is approximately the same. Referring to Equation (65), it follows by eliminating $f(x_E)$ that

$$\frac{\Delta h'_1}{\Delta h'_2} = \frac{h_1 - \Lambda}{h_2 - \Lambda},$$

where $\Delta h'_1$, $\Delta h'_2$ and h_1, h_2 are the values of $\Delta h'$ and corresponding values of $hcF2$ for the pair.

Then

$$\Lambda = \left[h_2 \frac{\Delta h'_1}{\Delta h'_2} - h_1\right] \Big/ \left[\frac{\Delta h'_1}{\Delta h'_2} - 1\right]. \tag{66}$$

This equation has been evaluated for ten cases selected from Fig. 21 and the results are given in Table XII. The median value of Λ is found to be 164 km., considerably higher than that obtained by Bradley and Dudeney. This may be significant because the Bradley and Dudeney model has too much ionization just above the E-layer maximum (see Fig. 12) where a semi-filled valley is known to exist.

It is to be noted that the mean value of Λ is also 164 km. with a standard error of 6 km.

Using this value of Λ, it is now possible to calculate $f(x_E)$ in Equation (65) as a function of x_E. The values thus generated are shown graphically in Fig. 22. It will be seen that there is now no discrepancy between

TABLE XII
RESULTS FROM EVALUATING EQUATION (66) USING DATA FROM FIG. 21

x_E	$hcF2$	$\Delta h'$	Λ
3·187	372	93	169
3·111	252	38	
3·138	367	118	161
3·167	259	56	
3·571	400	145	193
3·571	236	30	
3·639	427	121	153
3·641	262	48	
3·571	400	145	163
3·618	220	35	
4·091	361	84	184
4·100	283	47	
4·000	364	89	152
4·029	221	29	
2·687	328	132	124
2·712	246	79	
2·687	328	132	172
2·711	256	71	
2·687	328	132	166
2·657	252	70	
Median value			164
Mean value			164
Standard error in mean			6

the three seasonal groups of data. Also, $f(x_E)$ is clearly of a similar form to that used in the $\dot{hm}F2$ analysis, so that similar techniques can be used to evaluate it. Performing this analysis leads to the final result

$$\dot{ym}F2 = \dot{hm}F2 - h'F(F2) + \left[\frac{0\cdot93\pm0\cdot03}{(x_E-1\cdot23)} + (0\cdot05\pm0\cdot03)\right](\dot{hm}F2 - 164\pm6). \quad (67)$$

Following the procedure used on p. 36, the most probable uncertainty in y^*F2 is found to be

$$\overline{\delta\dot{ym}F2} = \pm\left\{\left[\left\{1\cdot05+\frac{0\cdot93}{(x_E-1\cdot23)}\right\}\delta\dot{hm}+0\cdot03(\dot{hm}-164)\left\{(x_E-1\cdot23)^{-1}+1\right\}\right]^2 + \left[\delta h'+\frac{558}{(x_E-1\cdot23)}+0\cdot03+\frac{0\cdot93(\dot{hm}-164)\,\delta x_E}{(x_E-1\cdot23)^2}\right]^2\right\}^{\frac{1}{2}}. \quad (68)$$

To obtain some idea of the manner in which this uncertainty varies with $\dot{hm}F2$ and with x_E, Equation (68) has been solved using the typical values: $\delta\dot{hm} = 10$ km., $\delta h' = 5$ km. (see Table IV), $\delta x_E/x_E = 0\cdot02$; for a range of x_E values and for $\dot{hm}F2$ between 200 and 400 km. It is found that the variation of $\overline{\delta\dot{ym}F2}$ as a function of $\dot{hm}F2$ at constant x_E (see Fig. 23) is approximately a straight line whose slope and intercept are functions of x_E. Note from the figure that the uncertainty in $\dot{ym}F2$ is a strong function of x_E at constant $\dot{hm}F2$, so much so that for $x_E < 1\cdot7$ the values of $ymF2$ derived from Equation (67) are meaningless. Even when x_E is greater than this limit, the equation produces no more than a rough guide to the value of

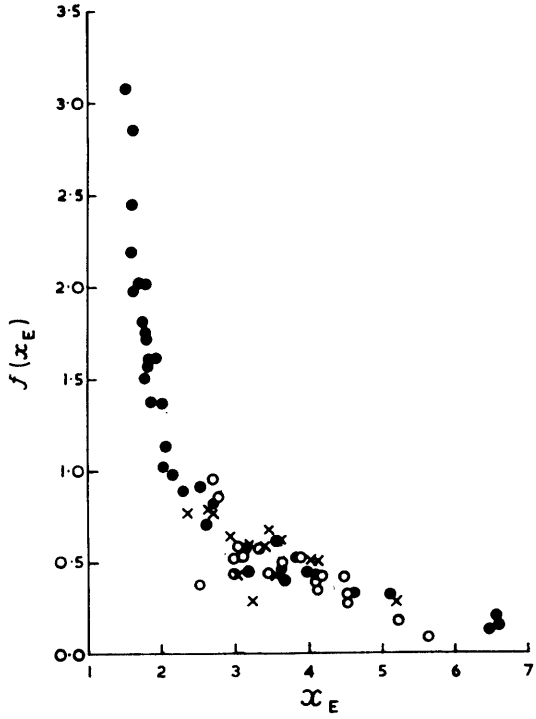

FIGURE 22

The data from Fig. 21 after normalization for changes in underlying slab thickness.

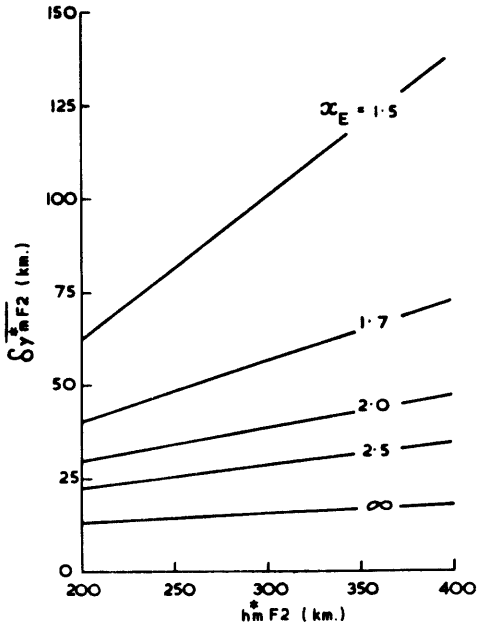

FIGURE 23

The uncertainty in the computed value of semi-thickness assuming a 10 km. error in $h\dot{m}$ and a 2 per cent error in x_E. $\delta y\dot{m}$ is given as a function of $h\dot{m}$, parametric in x_E.

ym. Clearly, a reduction in the uncertainties in $h\dot{m}F2$ and x_E would improve the situation but such a reduction would be difficult to obtain; the values used in the figure are close to the limit values for the type of ionogram under consideration.

This lack of precision in the determination of *ymF2* must of course apply in the case of the Bradley–Dudeney equation (Equation (41)) because of its similarity to Equation (67). However, it may be argued that *ymF2* itself has little physical significance at the very low values of x_E because the *F2*-layer nose in all probability does not follow a parabolic law under such conditions.

V. DISCUSSION

It is interesting to compare the empirical equation for *hmF2* developed here (Equation (56)) with that given by Bradley and Dudeney (see p. 23). The latter has been tested against true-height data from a number of widely spaced sites and its performance over the globe is therefore known. Fig. 24 shows the

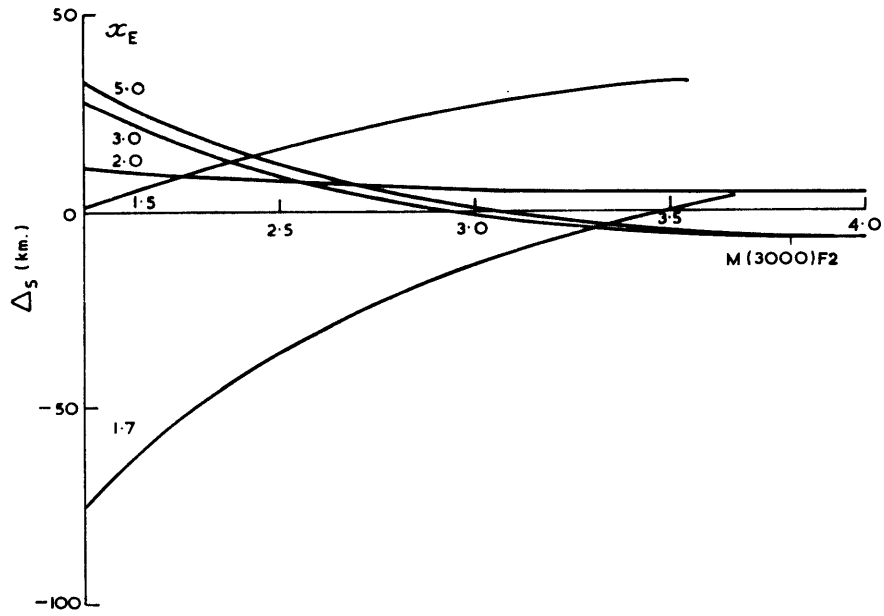

FIGURE 24

Comparison between Equation (56) and the Bradley–Dudeney equation. Δ_5 = *hmF2* (Equation 40)—*hmF2* (Equation 56). In the case $x_E = 1{\cdot}5$ the limit value of 1·7 has been used in Equation (40).

height difference Δ_5 obtained by subtracting *hmF2* given by Equation (56) from the value given by Equation (40) as a function of *M(3000)F2* for given values of x_E. The information contained in this figure is best brought out by considering the following three cases:

i. $x_E \geqslant 2{\cdot}0$; *M(3000)F2* $\geqslant 2{\cdot}6$. The values of Δ_5 are not significantly different from zero, bearing in mind the magnitude of the height uncertainties inherent in both equations (see for example Equation (63)) when used with routinely scaled data.

ii. $x_E < 2{\cdot}0$; all *M(3000)F2*. Δ_5 can be large positive or negative and varies greatly with both *M(3000)F2* and x_E. Clearly, for the true-height sample used in this report, the Bradley–Dudeney equation will give relatively poor results compared with those from Equation (56).

iii. $x_E \geqslant 2{\cdot}0$; *M(3000)F2* $\leqslant 2{\cdot}6$. For this case Δ_5 is positive and increases for all x_E as *M(3000)F2* decreases. Bradley and Dudeney (1973) pointed out that when *M(3000)F2* is below a limit value of between 2·4 and 2·7 (depending on geographical location) their equation consistently over-estimated *hmF2* by an amount which increased as *M(3000)F2* decreased. Fig. 24 therefore suggests that Equation (56), which gives lower values than Equation (40), will be less in error.

These points lead to the conclusion that Equation (56) is a better relationship for global use than is Equation (40); for, not only does it give better performance when *M(3000)F2* is low, but also it can be reliably used for values of x_E down to 1·5. However, the use of Equation (56) only removes about one-

third of the discrepancies found by Bradley and Dudeney for low values of *M(3000)F2*. The remainder probably results from one or both of two possible causes:

i. In practice, when *hṁF2* is very large (>500 km.), the profile shape at the frequencies where *M(3000)F2* is measured tends to be linear rather than parabolic. For a linear profile, *M(3000)F2* is not necessarily related to *hṁF2* (see also Bradley and Dudeney (1973)). This is a fundamental limitation in the application of any *M(3000)F2*-based equation.

ii. The empirical coefficients of Equation (54) (p. 31) are dependent on the dip and gyro-frequency of the magnetic field and therefore vary slowly with position. (This may be seen for example from Fig. 10 (p. 19) by comparing curve (b) with the dashed curve and bearing in mind that ΔM is essentially equivalent to $\Delta h'/ym$.) The magneto-ionic effects for a standard model profile (e.g. Bradley and Dudeney, 1973, fig. 12) could be established by computation. Alternatively, both magneto-ionic and physical changes with position could be evaluated using the techniques described in this report, applied to adequate samples of data from widely spaced observatories. Such an analysis should result in an empirical equation for *hṁF2* which is superior to either Equation (40) or Equation (56). However, it is questionable whether the improvement would warrant the effort required.

VI. SUMMARY AND CONCLUSIONS

THIS report describes a new simple method for reliably estimating *hmF2*. The method has considerable practical application because it relies only on the use of routinely scaled parameters. A novel way of correcting for group retardation in underlying layers, the "ΔM" correction factor, has proved to be a considerable improvement on existing schemes. The analysis has been presented in detail for the case of the Argentine Islands (lat. 65°15'S., long. 64°16'W.), but the techniques employed have a much wider application. The simplicity of the calibration procedure and of the final expressions means that the analysis can be carried out at field stations without the use of powerful computing facilities.

It is probable, though experimental verification is required, that the coefficients of the ΔM relation (Equation (54)) are functions of dip and gyro-frequency and vary only slowly with position. Comparison with the Bradley and Dudeney (1973) equation, which has been widely tested, show that it should be possible to use the same coefficients with confidence over quite wide zones.

Some examples of the applications of the scheme to the Argentine Islands data will be discussed in further reports.

VII. ACKNOWLEDGEMENTS

THE author gratefully acknowledges helpful discussions with Mr. W. R. Piggott of the British Antarctic Survey and Mr. P. A. Bradley of the S.R.C., Appleton Laboratory, Slough.

VIII. REFERENCES

APPLETON, E. V. *and* W. J. G. BEYNON. 1940. The application of ionospheric data to radio-communication problems: Part I. *Proc. phys. Soc.*, **52**, No. 4, 518–33.

————. *and* ————. 1947. The application of ionospheric data to radio-communication problems: Part II. *Proc. phys. Soc.*, **59**, No. 1, 58–76.

BECKER, W. 1960. Tables of ordinary and extraordinary refractive indices and $h'_{o,x}(f)$-curves for standard ionospheric layer models. *Mitt. Max-Planck-Inst. Aeronomie*, No. 4, 107 pp.

BOOKER, H. G. *and* S. L. SEATON. 1940. The relation between actual and virtual ionospheric height. *Phys. Rev.*, **57**, No. 1, 87–94.

BRADLEY, P. A. *and* J. R. DUDENEY. 1973. A simple model representation of the electron concentration of the ionosphere. *J. atmos. terr. Phys.*, **35**, No. 12, 2131–46.

BUDDEN, K. G. 1955. A method for determining the variation of electron density with height ($N(z)$ curves) from curves of equivalent height against frequency ($h'(f)$ curves). (*In Report of the Physical Society conference on the physics of the ionosphere, held at the Cavendish Laboratory, Cambridge, September* 1954. London, The Physical Society, 332–39.)

DECKER, R. P. 1972. Techniques for synthesizing median true height profiles from propagation parameters. *J. atmos. terr. Phys.*, **34**, No. 3, 451–64.

JACKSON, J. E. 1971. The $p'(f)$ to $N(h)$ inversion problem in ionospheric soundings. *GSFC Report*, No. X-625-71-186.

LAWRENCE, R. S., LITTLE, C. G. *and* H. J. A. CHIVERS. 1964. A survey of ionospheric effects upon Earth-space propagation. *Proc. Instn elect. Engrs*, **52**, No. 1, 4–27.

PIGGOTT, W. R. 1954. On the interpretation of the apparent ionisation distribution in the ionosphere. *J. atmos. terr. Phys.*, **5**, No. 4, 201–10.

———. *and* K. RAWER. 1972. *URSI handbook of ionogram interpretation and reduction.* 2nd edition. Washington, D.C., U.S. Department of Commerce. [N.O.A.A. Report UAG-23.]

RATCLIFFE, J. A. 1951. A quick method for analysing ionospheric records. *J. geophys. Res.*, **56**, No. 4, 463–85.

———. 1962. *The magneto-ionic theory and its application to the ionosphere. A monograph.* Cambridge, Cambridge University Press.

SCHMERLING, E. R. 1958. An easily applied method for the reduction of $h'(f)$ records to $N(h)$ profiles including the effects of the Earth's magnetic field. *J. atmos. terr. Phys.*, **12**, No. 1, 8–16.

———. 1967. Ten-point method of ionogram reduction. *Radio Sci.*, **2**, No. 10, 1233–36.

SHIMAZAKI, T. 1955. Worldwide variations in the height of the maximum electron density in the ionospheric *F2*-layer. *J. Radio Res. Labs Japan*, **2**, No. 7, 85–97.

SMITH, N. 1937. Extension of normal incidence ionospheric measurements to oblique incidence. *Bur. Stand. J. Res.*, **19**.

———. 1939. The relation of radio sky-wave transmission to ionosphere measurements. *Proc. Inst. Radio Engrs*, **27**, No. 5, 332–47.

TAIEB, C. 1967. A quick model method for obtaining real height parameters from routine ionospheric data. *Radio Sci.*, **2**, No. 10, 1263–67.

VICKERS, M. D. 1959. The effect of the *F1*-layer on the calculation of the height of the *F2*-layer. *J. atmos. terr. Phys.*, **16**, No. 2, 103–05.

WRIGHT, J. W. *and* R. E. MCDUFFIE. 1960. The relation of *hmF2* to *M(3000)F2* and *hpF2*. *J. Radio Res. Labs Japan*, **7**, No. 32, 409–17.